

# A Reduced Augmentation Implicit Low-rank (RAIL) integrator for solving three-dimensional diffusion and advection-diffusion equations in the Tucker tensor format

Joseph Nakao · Gianluca Ceruti · Lukas Einkemmer

**Abstract** This paper presents a rank-adaptive implicit integrator for the tensor solution of three-dimensional diffusion and advection-diffusion equations. In particular, the recently developed Reduced Augmentation Implicit Low-rank (RAIL) integrator is extended from two-dimensional matrix solutions to three-dimensional tensor solutions stored in a Tucker tensor decomposition. Spectral methods are considered for spatial discretizations, and diagonally implicit Runge-Kutta (RK) and implicit-explicit (IMEX) RK methods are used for time discretization. The RAIL integrator first discretizes the partial differential equation fully in space and time. Then at each RK stage, the bases computed at the previous stages are augmented and reduced to predict the current (future) basis and construct projection subspaces. After updating the bases in a dimension-by-dimension manner, a Galerkin projection is performed by projecting onto the span of the previous bases and the newly updated bases. A truncation procedure according to a specified tolerance follows. Numerical experiments demonstrate the accuracy of the integrator using implicit and implicit-explicit time discretizations, as well as how well the integrator captures the rank of the solutions.

**Keywords:** low-rank, Basis Update and Galerkin (BUG), Tucker decomposition, implicit-explicit method, advection-diffusion equation

**Mathematics Subject Classification:** 65M06

## 1 Introduction

The use of low-rank ansatzes has gained significant traction in recent years, driven by their ability to efficiently tackle high-dimensional computational problems in various scientific and engineering disciplines. By exploiting inherent structure and reducing computational complexity, low-rank approaches have become indispensable in areas such as numerical linear algebra, data science, and the simulation of physical systems. However, this challenge becomes even more pronounced when dealing with time-dependent problems, where the low-rank decomposition must be computed repeatedly at each time step, leading to significantly increased demands on computational resources.

While approaches based on the Proper Orthogonal Decomposition (POD), where snapshots of the dynamics are computed and subsequently compressed offline to obtain a reduced-order model of the system, have been successfully applied in various contexts, an alternative approach has emerged over the

---

J. Nakao

Department of Mathematics and Statistics, Swarthmore College, Swarthmore, PA, USA

E-mail: jnakao1@swarthmore.edu

ORCID: 0009-0008-6589-4013

G. Ceruti

Department of Mathematics, University of Innsbruck, Innsbruck, Tyrol, Austria

E-mail: gianluca.ceruti@uibk.ac.at

ORCID: 0009-0009-2644-8093

L. Einkemmer

Department of Mathematics, University of Innsbruck, Innsbruck, Tyrol, Austria

E-mail: lukas.einkemmer@uibk.ac.at

ORCID: 0000-0002-8798-2304

past decade. In this new approach, the low-rank decomposition is performed instantaneously, with the reduced space describing the system dynamics being updated at each time step – we refer to [18] for a systematic review of the kinetic setting.

In this novel framework, several numerical strategies have recently emerged. A natural first approach, often referred to as Step-And-Truncate (SAT), involves fully discretizing the dynamics in both space and time, followed by a truncation procedure at the end of each time-step to maintain a low-rank solution [14, 16, 26, 27, 34, 52, 54, 55]. This method is appealing for its simplicity but often requires corrections to account for the physical constraints of the problem. Although SAT shows great potential, the size of the basis (due to the time-step) greatly increases and demands truncation, which in turn can lead to significant memory and computational cost. This overhead can be mitigated using techniques like the Discrete Empirical Interpolation Method (DEIM), as demonstrated in pioneering works such as [11, 15, 23]. Extensions to this line of research include the use of randomized projections, as proposed in [39].

An alternative approach involves geometric methods such as the Dynamical Low-Rank (DLR) approximation [31]. Here, the discretized solution is decomposed into time-dependent factor matrices describing the one-dimensional spatial bases, and a core tensor (matrix in the two-dimensional case) carrying time-dependent coefficients describing the interactions among the bases. The set of low-rank matrices is treated as a manifold, and the dynamics are approximated locally in its tangent space. This approach introduces additional stiffness into the system due to the local geometric approximation, and substantial research has focused on developing robust numerical integrators to address this issue, collectively known as the Projector-Splitting Integrator (PSI) [42] and Basis-Update and Galerkin approximation (BUG) integrators [5–7]. Furthermore, DEIM and randomized techniques have recently been incorporated into these numerical schemes, as proposed in [4, 12, 22, 46], to enhance computational efficiency and fidelity.

The class of robust DLR integrators, such as BUG, has paved an insightful path for applying low-rank techniques to high-dimensional time-dependent problems. However, this class of methods revealed several challenges. First, due to the inherently local first-order geometric approximation underlying DLR methods, the original robust numerical integrators were mostly limited to first-order accuracy in time. Second, while matrix-based low-rank techniques suffice for many applications, problems arising in fields such as molecular quantum dynamics or plasma physics often necessitate low-rank representations in higher dimensions. As such, low-rank tensor decompositions are required to store the solution, including Tucker tensors, tensor trains, or hierarchical formats [25, 33].

Addressing time-order convergence, numerous studies have extended BUG integrators to achieve second-order [9, 38, 57] and even higher-order accuracy [49]. These higher-order methods typically employ explicit time discretizations, whereas systems with severe stiffness require the use of implicit integrators. Several recent works have presented implicit low-rank integrators to address this issue in the matrix case [1, 13, 17, 19–21, 41, 45, 47, 48, 53, 56, 59]. In [48], a Reduced Augmentation Implicit Low-rank (RAIL) approach was proposed for solving two-dimensional advection-diffusion equations, in which the bases computed at previous Runge-Kutta stages were efficiently augmented to form a low-rank projection space that allowed for high-order accuracy to be observed in various numerical experiments using implicit and implicit-explicit Runge-Kutta methods. Addressing high-dimensional extensions, the application of low-rank ansatzes such as Tucker tensors has been extensively pursued in related DLR techniques [8, 32, 43, 44]. Despite the significant progress that has been made to address these two challenges, there remains a need for low-rank integrators that are implicit, high-order accurate in time, and can accommodate high-dimensional problems in tensor format.

In this paper, we focus on the extension and analysis of the RAIL technique within the framework of the three-dimensional Tucker tensor decomposition. Following a close analogy to the original RAIL formulation in [48], our goal is to efficiently address the computational challenges posed by solving three-dimensional advection-diffusion equations of the form:

$$u_t + \nabla \cdot (\mathbf{a}(\mathbf{x}, t)u) = \nabla \cdot (\mathbf{D}\nabla u) + c(\mathbf{x}, t), \quad \mathbf{x} \in \Omega \subset \mathbb{R}^3, \quad t > 0, \quad (1)$$

where  $\mathbf{a}(\mathbf{x}, t)$  describes a flow field,  $\mathbf{D}$  is a diagonal diffusion tensor, and  $c(\mathbf{x}, t)$  is a source term. We assume that the solution, flow field and source term can all be well approximated by low-rank functions. Under this assumption, the low-rank structures can be exploited to reduce the storage requirements of the numerical solution and enhance computational efficiency.

The present manuscript is organized as follows. In Section 2, we recall preliminaries on tensor notation and definitions, along with a recap of the Tucker decomposition for third-order Tucker tensors. Additionally, we revisit the efficient solver from [58] for Tucker tensor equations. In Section 3, we introduce the RAIL-3D scheme using diagonally implicit Runge-Kutta schemes for the diffusive component only, accompanied by a consistency and stability analysis. Section 4 further incorporates the advection

component and explores the application of implicit-explicit Runge-Kutta schemes. Finally, in Section 5, we present several numerical experiments that demonstrate the effectiveness of the proposed RAIL-3D scheme.

## 2 Preliminaries

We begin by briefly reviewing three key topics that will help introduce the RAIL-3D integrator: (1) tensor notation and definitions, (2) the Tucker decomposition of a third-order tensor, and (3) a direct solver for third-order tensor linear equations [58]. For the first two subsections on tensors, we summarize key concepts and refer the reader to the comprehensive review paper by Kolda and Bader on tensor decompositions [33].

### 2.1 Tensor notation and definitions

Throughout this paper, we follow the notation used in [33]. Vectors (first order tensors/one-dimensional arrays) are denoted by boldface lowercase letters, e.g.,  $\mathbf{a}$ . Matrices (second order tensors/two-dimensional arrays) are denoted by boldface uppercase letters, e.g.,  $\mathbf{A}$ . Third order tensors/three-dimensional arrays are denoted by boldface Euler script letters, e.g.,  $\mathcal{A}$ . We only concern ourselves with at most third-order tensors since the present paper applies tensors to efficiently solve the three-dimensional equation (1). We refer the reader to the review papers [33] and [25] for a systematic review of various tensor decompositions.

In this manuscript, three-way tensors naturally emerge from the discretization of the 3D solution to advection-diffusion equations by considering a scalar function  $u(x, y, z)$  and uniform computational grids in each dimension,

$$x_1 < x_2 < \dots < x_{N_x}, \quad y_1 < y_2 < \dots < y_{N_y}, \quad z_1 < z_2 < \dots < z_{N_z}. \quad (2)$$

The function  $u(x, y, z)$  is discretized over the tensor product of these uniform computational grids and stored in a three-dimensional array, or rather, third-order tensor,  $\mathcal{U} \in \mathbb{R}^{N_x \times N_y \times N_z}$ . The elements of  $\mathcal{U}$  are denoted by  $u_{ijk} \approx u(x_i, y_j, z_k)$ , for  $i = 1, \dots, N_x$ ,  $j = 1, \dots, N_y$  and  $k = 1, \dots, N_z$ . Before proceeding any further, we first recall a few definitions that will help prepare the reader for the remainder of this paper.

**Definition 1 (Mode- $n$  fibers)** The fibers of a tensor are defined by fixing all but a single index. In particular, the collection of mode- $n$  fibers fix all but the  $n$ th index.

**Definition 2 (Mode- $n$  matricization)** The mode- $n$  matricization, also known as the mode- $n$  unfolding or flattening, of a tensor  $\mathcal{U}$  is defined by the matrix  $\mathbf{U}_{(n)}$  whose columns are the mode- $n$  fibers of  $\mathcal{U}$ . In the case of a third order tensor  $\mathcal{U} \in \mathbb{R}^{N_x \times N_y \times N_z}$ , note that  $\mathbf{U}_{(1)} \in \mathbb{R}^{N_x \times N_y N_z}$ ,  $\mathbf{U}_{(2)} \in \mathbb{R}^{N_y \times N_x N_z}$  and  $\mathbf{U}_{(3)} \in \mathbb{R}^{N_z \times N_x N_y}$ . We note that the arrangement of mode- $n$  fibers does not matter as long as it is applied consistently.

**Definition 3 (Vectorization)** The vectorization of a third order tensor  $\mathcal{U} \in \mathbb{R}^{N_x \times N_y \times N_z}$ , denoted  $\text{vec}(\mathcal{U}) \in \mathbb{R}^{N_x N_y N_z}$ , is the column vector defined by stacking all of the mode- $n$  fibers. Similar to the mode- $n$  matricization, the choice of  $n$  and the order in which the fibers are arranged do not matter as long as the process is consistently used.

**Definition 4 (Norm of a tensor)** The norm  $\|\cdot\|$  of a (third order) tensor  $\mathcal{U} \in \mathbb{R}^{N_x \times N_y \times N_z}$  is defined as the square root of the sum of the square of all its elements. That is,

$$\|\mathcal{U}\| := \sqrt{\sum_{i=1}^{N_x} \sum_{j=1}^{N_y} \sum_{k=1}^{N_z} u_{ijk}^2}. \quad (3)$$

**Definition 5 (Hadamard product)** The Hadamard product of two (third order) tensors  $\mathcal{A}$  and  $\mathcal{B}$ , denoted by  $\mathcal{A} * \mathcal{B}$ , is the elementwise product of their corresponding entries. The elements of  $\mathcal{X} = \mathcal{A} * \mathcal{B}$  are  $x_{ijk} = a_{ijk} b_{ijk}$ , for  $i = 1, \dots, N_x$ ,  $j = 1, \dots, N_y$  and  $k = 1, \dots, N_z$ .

**Definition 6 (Kronecker product for matrices)** The Kronecker product of two matrices  $\mathbf{A} \in \mathbb{R}^{I \times J}$  and  $\mathbf{B} \in \mathbb{R}^{P \times Q}$ , denoted by  $\mathbf{A} \otimes \mathbf{B} \in \mathbb{R}^{IP \times JQ}$ , is the matrix defined by

$$\mathbf{A} \otimes \mathbf{B} = \begin{pmatrix} a_{11}\mathbf{B} & \dots & a_{1J}\mathbf{B} \\ a_{21}\mathbf{B} & \dots & a_{2J}\mathbf{B} \\ \vdots & \ddots & \vdots \\ a_{I1}\mathbf{B} & \dots & a_{IJ}\mathbf{B} \end{pmatrix} = \left[ \mathbf{a}_{:,1} \otimes \mathbf{b}_{:,1} \mid \mathbf{a}_{:,1} \otimes \mathbf{b}_{:,2} \mid \mathbf{a}_{:,1} \otimes \mathbf{b}_{:,3} \mid \dots \mid \mathbf{a}_{:,J} \otimes \mathbf{b}_{:,Q-1} \mid \mathbf{a}_{:,J} \otimes \mathbf{b}_{:,Q} \right]. \quad (4)$$

We recall two properties of the Kronecker product:

*Property 1*  $\mathbf{AB} \otimes \mathbf{CD} = (\mathbf{A} \otimes \mathbf{C})(\mathbf{B} \otimes \mathbf{D})$ .

*Property 2*  $\text{vec}(\mathbf{AXB}^T) = (\mathbf{B} \otimes \mathbf{A})\text{vec}(\mathbf{X})$ .

**Definition 7 (Kronecker product for third order tensors)** The Kronecker product of two (third order) tensors  $\mathcal{A} \in \mathbb{R}^{I \times J \times K}$  and  $\mathcal{B} \in \mathbb{R}^{P \times Q \times R}$  is denoted  $\mathcal{A} \otimes \mathcal{B}$ , with a slight abuse of notation. The resulting tensor  $\mathcal{X} = \mathcal{A} \otimes \mathcal{B}$  is a third-order tensor of size  $IP \times JQ \times KR$  with a block tensor structure, where each block consists of the third-order tensors  $a_{ijk}\mathcal{B}$  for  $i = 1, \dots, I$ ,  $j = 1, \dots, J$ , and  $k = 1, \dots, K$ . The blockwise elements are given by

$$(\mathcal{X})_{(i-1)P+1:iP, (j-1)Q+1:jQ, (k-1)R+1:kR} = a_{ijk}\mathcal{B}, \quad i = 1, \dots, I, \quad j = 1, \dots, J, \quad k = 1, \dots, K. \quad (5)$$

Throughout this paper, it should be clear from context whether  $\otimes$  denotes the matrix Kronecker product or the tensor Kronecker product. Although the matrix Kronecker product is more commonly known, the tensor Kronecker product is less so. We refer the reader to [51] for a thorough treatment of this topic and structured tensor computations.

**Definition 8 (Kronecker sum for square matrices)** The Kronecker sum of two square matrices  $\mathbf{A} \in \mathbb{R}^{P \times P}$  and  $\mathbf{B} \in \mathbb{R}^{Q \times Q}$ , denoted  $\mathbf{A} \oplus \mathbf{B} \in \mathbb{R}^{PQ \times PQ}$ , is the matrix defined by

$$\mathbf{A} \otimes \mathbf{I}_{Q \times Q} + \mathbf{I}_{P \times P} \otimes \mathbf{B}, \quad (6)$$

where  $\mathbf{I}_{P \times P}$  and  $\mathbf{I}_{Q \times Q}$  are the identity matrices of sizes  $P \times P$  and  $Q \times Q$ , respectively. Note that this is different from the direct sum of matrices which uses the same notation  $\oplus$ .

**Definition 9 (Khatri-Rao product)** The Khatri-Rao product of two matrices  $\mathbf{A} \in \mathbb{R}^{I \times K}$  and  $\mathbf{B} \in \mathbb{R}^{J \times K}$ , denoted by  $\mathbf{A} \odot \mathbf{B} \in \mathbb{R}^{IJ \times K}$ , is the matrix defined by

$$\mathbf{A} \odot \mathbf{B} = \left[ \mathbf{a}_{:,1} \otimes \mathbf{b}_{:,1} \mid \mathbf{a}_{:,2} \otimes \mathbf{b}_{:,2} \mid \dots \mid \mathbf{a}_{:,K} \otimes \mathbf{b}_{:,K} \right]. \quad (7)$$

**Definition 10 (Tensor mode- $n$  product)** Consider a third order tensor  $\mathcal{U} \in \mathbb{R}^{N_x \times N_y \times N_z}$  and matrices  $\mathbf{V}_x \in \mathbb{R}^{N'_x \times N_x}$ ,  $\mathbf{V}_y \in \mathbb{R}^{N'_y \times N_y}$  and  $\mathbf{V}_z \in \mathbb{R}^{N'_z \times N_z}$ . The mode-1 product between the tensor  $\mathcal{U}$  and the matrix  $\mathbf{V}_x$ , denoted  $\mathcal{U} \times_1 \mathbf{V}_x$ , is a tensor of size  $N'_x \times N_y \times N_z$ . Elementwise,

$$(\mathcal{U} \times_a \mathbf{V}^x)_{i'jk} = \sum_{i=1}^{N_x} u_{ijk} v_{i'}^x, \quad i' = 1, \dots, N'_x, \quad j = 1, \dots, N_y, \quad k = 1, \dots, N_z. \quad (8)$$

Equivalently stated, the mode-1 product between  $\mathcal{U}$  and  $\mathbf{V}_x$  multiplies each mode-1 fiber of  $\mathcal{U}$  by the matrix  $\mathbf{V}_x$ . In the matricized form, the mode-1 products between  $\mathcal{U}$  and  $\mathbf{V}_x$ ,  $\mathcal{U}$  and  $\mathbf{V}_y$ , and  $\mathcal{U}$  and  $\mathbf{V}_z$  are respectively

$$\mathcal{X} = \mathcal{U} \times_1 \mathbf{V}_x \quad \Leftrightarrow \quad \mathbf{X}_{(1)} = \mathbf{V}_x \mathbf{U}_{(1)}. \quad (9a)$$

$$\mathcal{Y} = \mathcal{U} \times_2 \mathbf{V}_y \quad \Leftrightarrow \quad \mathbf{Y}_{(2)} = \mathbf{V}_y \mathbf{U}_{(2)}, \quad (9b)$$

$$\mathcal{Z} = \mathcal{U} \times_3 \mathbf{V}_z \quad \Leftrightarrow \quad \mathbf{Z}_{(3)} = \mathbf{V}_z \mathbf{U}_{(3)}. \quad (9c)$$

We note that the order of mode- $n$  products is irrelevant in a series of multiplications if the modes are distinct. That is,

$$\mathcal{U} \times_n \mathbf{A} \times_m \mathbf{B} = \mathcal{U} \times_m \mathbf{B} \times_n \mathbf{A} \quad \text{if } n \neq m. \quad (10)$$

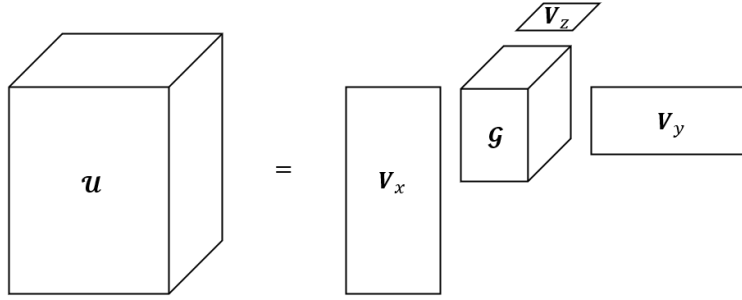


Fig. 1: Tucker decomposition of a third order tensor.

## 2.2 Tucker decomposition of a third order tensor

Due to its cubic storage complexity  $\mathcal{O}(N^3)$ , directly working with the full tensor  $\mathcal{U}$  becomes impractical for large  $N$ , where we assume  $N = N_x = N_y = N_z$ . Such a situation naturally arises, for example, when using an extremely fine grid which necessitates a large  $N$ . Thus, just as a matrix can be decomposed and approximated using a low-rank representation obtained from a truncated singular value decomposition (SVD), a tensor can be treated similarly. Although various tensor decompositions exist, we here focus on the high-dimensional analogue of the SVD: the Tucker decomposition. This decomposition is also known as the higher-order SVD (HOSVD) or higher-order principal component analysis. The Tucker decomposition of a third-order tensor was originally proposed in [61, 62] and extended to higher-order tensors in [30].

The Tucker decomposition decomposes a third order tensor  $\mathcal{U}$  into a (smaller) *core tensor* which is multiplied by a matrix along each dimension using the mode- $n$  product from Definition 10. This is seen in Figure 1 in which the core tensor is  $\mathcal{G}$ , and the matrices multiplying the core tensor (also called the *factor matrices*) are  $\mathbf{V}_x, \mathbf{V}_y, \mathbf{V}_z$ . Although the factor matrices need not be orthonormal, this is usually desired. The Tucker decomposition of a third order tensor  $\mathcal{U}$  is represented by

$$\mathcal{U} = \mathcal{G} \times_1 \mathbf{V}_x \times_2 \mathbf{V}_y \times_3 \mathbf{V}_z. \quad (11)$$

The core tensor is size  $r_x \times r_y \times r_z$ , and the factor matrices are sizes  $N_x \times r_x$ ,  $N_y \times r_y$ , and  $N_z \times r_z$ , respectively. Since the number of column vectors in each factor matrix is typically different, we say that the *multilinear rank* of the tensor  $\mathcal{U}$  is the 3-tuple  $(r_x, r_y, r_z)$ . Ideally,  $r_x \ll N_x$ ,  $r_y \ll N_y$  and  $r_z \ll N_z$  so that the storage complexity is significantly reduced. In particular, the storage complexity of a Tucker decomposition is  $\mathcal{O}(r^3 + dNr)$ , a significant reduction from  $\mathcal{O}(N^3)$  if the tensor admits a small multilinear rank. In application, the main objective is to obtain a low-multilinear rank Tucker decomposition that closely approximates the original third-order tensor.

The factor matrices can be interpreted as one-dimensional bases with respect to each variable. Whereas, the core tensor can be interpreted as representing the amount of interaction between the one-dimensional basis vectors. However, it's important to note that the entries of the core tensor should not be thought of analogously to singular values. Unlike the singular values of a matrix, the entries of the core tensor could be negative and are not necessarily ordered, and the core tensor is generally dense. Nonetheless, under the low-rank assumption, the Tucker decomposition for third-order tensors represents an incredibly useful tool for potentially reducing the storage complexity and for decomposing a function  $u(x, y, z)$  into its one-dimensional components. The mode- $n$  matricizations (and vectorization) for the Tucker decomposition (11) are respectively

$$\mathbf{U}_{(1)} = \mathbf{V}_x \mathbf{G}_{(1)} (\mathbf{V}_z \otimes \mathbf{V}_y)^T = \mathbf{V}_x \mathbf{G}_{(1)} (\mathbf{V}_z^T \otimes \mathbf{V}_y^T), \quad (12a)$$

$$\mathbf{U}_{(2)} = \mathbf{V}_y \mathbf{G}_{(2)} (\mathbf{V}_z \otimes \mathbf{V}_x)^T = \mathbf{V}_y \mathbf{G}_{(2)} (\mathbf{V}_z^T \otimes \mathbf{V}_x^T), \quad (12b)$$

$$\mathbf{U}_{(3)} = \mathbf{V}_z \mathbf{G}_{(3)} (\mathbf{V}_y \otimes \mathbf{V}_x)^T = \mathbf{V}_z \mathbf{G}_{(3)} (\mathbf{V}_y^T \otimes \mathbf{V}_x^T), \quad (12c)$$

$$\text{vec}(\mathcal{U}) = (\mathbf{V}_z \otimes \mathbf{V}_y \otimes \mathbf{V}_x) \text{vec}(\mathcal{G}). \quad (12d)$$

A natural question arises: how can we obtain a truncated Tucker decomposition of a third-order tensor? In the matrix case, one can simply truncate the singular values based on a specified tolerance to obtain the optimal low-rank approximation. However, for third-order tensors, various algorithms exist for

computing a low-multilinear rank Tucker decomposition that approximates the original tensor; see [33] for a list of references. In the present paper, we use the *truncated high-order SVD (HOSVD)* algorithm from [10] which produces a Tucker decomposition of a specified multilinear rank  $(\tilde{r}_1, \tilde{r}_2, \tilde{r}_3)$ . Simply put, the truncated HOSVD takes the first  $\tilde{r}_n$  left singular vectors of the matricization  $\mathbf{U}_{(n)}$ ; note that the factor matrices are orthonormal. Then, the mode- $n$  products between  $\mathcal{U}$  and the transposed factor matrices can be used to construct the core tensor. Alternatively, a specified tolerance on the residual can be used to determine the truncated HOSVD. The truncated HOSVD does not typically produce an optimal approximation, but it does satisfy the error bound given in Theorem 1.

**Theorem 1 ([10, 34])** *Let  $\mathcal{U} \in \mathbb{R}^{N_1 \times N_2 \times N_3}$  be a third order tensor, and let  $\tilde{\mathcal{U}} \in \mathbb{R}^{N_1 \times N_2 \times N_3}$  be the truncated Tucker tensor of multilinear rank  $(\tilde{r}_1, \tilde{r}_2, \tilde{r}_3)$  resulting from the truncated HOSVD. Let  $\mathcal{T}(\tilde{r}_1, \tilde{r}_2, \tilde{r}_3)$  denote the set of Tucker tensors of multilinear rank  $(\tilde{r}_1, \tilde{r}_2, \tilde{r}_3)$ . Then, the following error bound holds:*

$$\left\| \mathcal{U} - \tilde{\mathcal{U}} \right\| \leq \sqrt{3} \min_{\mathcal{X} \in \mathcal{T}(\tilde{r}_1, \tilde{r}_2, \tilde{r}_3)} \left\| \mathcal{U} - \mathcal{X} \right\|. \quad (13)$$

Due to its usefulness later on, we also present the following result on the Tucker decomposition of the Hadamard product of two tensors in Tucker tensor format.

**Theorem 2 (Tucker decomposition of the Hadamard product of two Tucker tensors [40])**

*Let  $\mathcal{X} = \mathcal{G}^x \times_1 \mathbf{A}_1 \times_2 \mathbf{A}_2 \times_3 \mathbf{A}_3$  and  $\mathcal{Y} = \mathcal{G}^y \times_1 \mathbf{B}_1 \times_2 \mathbf{B}_2 \times_3 \mathbf{B}_3$  be third-order Tucker tensors of size  $N_1 \times N_2 \times N_3$ , and with respective multilinear ranks  $(r_1^{(x)}, r_2^{(x)}, r_3^{(x)})$  and  $(r_1^{(y)}, r_2^{(y)}, r_3^{(y)})$ . Then, it holds that*

$$\mathcal{X} * \mathcal{Y} = (\mathcal{G}^x \otimes \mathcal{G}^y) \times_1 (\mathbf{A}_1 \odot^T \mathbf{B}_1) \times_2 (\mathbf{A}_2 \odot^T \mathbf{B}_2) \times_3 (\mathbf{A}_3 \odot^T \mathbf{B}_3), \quad (14)$$

where  $\odot^T$  is the transpose Khatri-Rao product defined as

$$\mathbf{A} \odot^T \mathbf{B} := (\mathbf{A}^T \odot \mathbf{B}^T)^T = \left[ \mathbf{a}_{1,:}^T \otimes \mathbf{b}_{1,:}^T, \dots, \mathbf{a}_{N,:}^T \otimes \mathbf{b}_{N,:}^T \right]^T = \begin{bmatrix} (\mathbf{a}_{1,:}^T \otimes \mathbf{b}_{1,:}^T)^T \\ \dots \\ (\mathbf{a}_{N,:}^T \otimes \mathbf{b}_{N,:}^T)^T \end{bmatrix} = \begin{bmatrix} \mathbf{a}_{1,:} \otimes \mathbf{b}_{1,:} \\ \dots \\ \mathbf{a}_{N,:} \otimes \mathbf{b}_{N,:} \end{bmatrix}. \quad (15)$$

The proof of equation (14) in Theorem 2 can be found in [40]. Note that the multilinear rank of  $\mathcal{X} * \mathcal{Y}$  is  $(r^2, r^2, r^2)$  assuming the same rank  $r$  for the sake of analyzing the storage complexity. If the multilinear rank of either  $\mathcal{X}$  or  $\mathcal{Y}$  is too large, this can quickly become expensive and would require further compression to maintain efficiency; such algorithms are summarized in [35].

*Remark 1* We remind the reader that for order- $d$  tensors in higher dimensions, the storage complexity of the Tucker decomposition is  $\mathcal{O}(r^d + dNr)$ . Other low-rank tensor decompositions offer alternative ways to store the tensor solution, e.g., tensor train [50], and hierarchical Tucker/tree tensor networks [25, 28]. In general, these other tensor decompositions are more advantageous for  $d \geq 4$  since their storage complexities are often dominated by a  $\mathcal{O}(r^3)$  term for low-rank tensors. Thus, in three dimensions, the storage complexity of the Tucker decomposition is comparable to that of these alternative decompositions, making it a suitable choice for the proposed framework.

### 2.3 A third-order tensor linear equation solver

We summarize the direct solver from [58] for efficiently solving third-order tensor linear equations of the form

$$(\mathbf{M}_1 \otimes \mathbf{A}_1 \otimes \mathbf{H} + \mathbf{A}_2 \otimes \mathbf{M} \otimes \mathbf{H} + \mathbf{H}_3 \otimes \mathbf{M} \otimes \mathbf{A}_3) \text{vec}(\mathcal{X}) = \text{vec}(\mathcal{B}), \quad (16)$$

where all the coefficient matrices are real and have the same  $N \times N$  dimensions,  $\mathcal{B}$  is a low-rank, and  $\mathbf{M}, \mathbf{H}, \mathbf{M}_1, \mathbf{H}_3, \mathcal{A} = \mathbf{M}_1 \otimes \mathbf{A}_1 \otimes \mathbf{H} + \mathbf{A}_2 \otimes \mathbf{M} \otimes \mathbf{H} + \mathbf{H}_3 \otimes \mathbf{M} \otimes \mathbf{A}_3$  are nonsingular.

There are many iterative methods for efficiently solving equation (16) that exploit Kronecker and low-rank structures of the iteration matrices [36, 37]. However, the algorithm presented in [58] offers an alternative method that is particularly ideal for our situation since it is a direct solver, straightforward to understand, and easy to implement. Moreover, it does not require the use of the coefficient matrix in Kronecker form. As mentioned in [58], this direct solver can serve as a workhorse for solving reduced equations that show up in projection based procedures for large and sparse third order tensor equations, such as the proposed implicit integrator. We emphasize that this algorithm is specifically designed for solving third-order tensor linear equations. For higher-order tensor linear equations, iterative methods might be a more suitable choice. Moreover, we emphasize that although the algorithm in [58] is presented

for rank-1 righthand sides of the form  $\mathcal{B} = \mathbf{b}_1 \otimes \mathbf{b}_2 \otimes \mathbf{b}_3$ , it can be easily extended to general (low-rank) third-order tensors  $\mathcal{B}$ . We thus present this extension as Corollary 1 and provide its proof for completeness. The proof is constructive, and with the exception of the righthand being a general third-order tensor, is identical to the proof of Theorem 2.1 in [58]. The algorithm for the direct solver follows naturally from its constructive proof. Simoncini includes MATLAB code for the rank-1 case in [58]; for the extended case, small obvious modifications just need to be made.

**Corollary 1 (Extension of Theorem 2.1 in [58])** *Let  $\mathbf{A}_3^T \mathbf{H}^{-T} = \mathbf{Q} \mathbf{R} \mathbf{Q}^*$  be the Schur decomposition of  $\mathbf{A}_3^T \mathbf{H}^{-T}$ , and  $[\mathbf{g}_1, \dots, \mathbf{g}_N] := \mathbf{B}_{(1)}^T \mathbf{H}^{-T} \mathbf{Q}$ . Using the mode-1 matricization, the solution  $\mathcal{X}$  to equation (16) is given by*

$$\mathbf{X}_{(1)} = \mathbf{Q}[\hat{\mathbf{z}}_1, \dots, \hat{\mathbf{z}}_N]^T \in \mathbb{R}^{N \times N^2}, \quad (17)$$

where for  $j = 1, \dots, N$ , the vector  $\hat{\mathbf{z}}_j = \text{vec}(\hat{\mathbf{Z}}_j)$  is the vectorization of the matrix  $\hat{\mathbf{Z}}_j$  that solves the Sylvester equation

$$\mathbf{M}^{-1} \mathbf{A}_1 \mathbf{Z} + \mathbf{Z}(R_{j,j} \mathbf{H}_3^T \mathbf{M}_1^{-T} + \mathbf{A}_2^T \mathbf{M}_1^{-T}) = (\mathbf{M}^{-1} \mathbf{G}_j - \mathbf{W}_{j-1} \mathbf{H}_3^T) \mathbf{M}_1^{-T}, \quad (18)$$

where  $R_{j,j}$  denotes the  $(j, j)$  element of the upper triangular matrix  $\mathbf{R}$ ,  $\mathbf{G}_j$  is the matrix such that  $\mathbf{g}_j = \text{vec}(\mathbf{G}_j)$ , and  $\mathbf{W}_{j-1}$  is the matrix such that  $\mathbf{w}_{j-1} = \text{vec}(\mathbf{W}_{j-1})$  with  $\mathbf{w}_{j-1} = [\hat{\mathbf{z}}_1, \dots, \hat{\mathbf{z}}_{j-1}] R_{1:j-1, j}$ . We define  $\mathbf{W}_0$  to be an empty array for  $j = 1$ .

*Proof* Equation (16) can be written as

$$\mathcal{X} \times_1 \mathbf{H} \times_2 \mathbf{A}_1 \times_3 \mathbf{M}_1 + \mathcal{X} \times_1 \mathbf{H} \times_2 \mathbf{M} \times_3 \mathbf{A}_2 + \mathcal{X} \times_1 \mathbf{A}_3 \times_2 \mathbf{M} \times_3 \mathbf{H}_3 = \mathcal{B}, \quad (19)$$

which after performing the mode-1 matricization can be written as

$$\mathbf{H} \mathbf{X}_{(1)} (\mathbf{A}_2 \otimes \mathbf{M} + \mathbf{M}_1 \otimes \mathbf{A}_1)^T + \mathbf{A}_3 \mathbf{X}_{(1)} (\mathbf{H}_3 \otimes \mathbf{M})^T = \mathbf{B}_{(1)}. \quad (20)$$

Multiplying equation (20) on the left by  $\mathbf{H}^{-1}$  and on the right by  $\mathbf{H}_3^{-T} \otimes \mathbf{M}^{-T}$ , and letting  $\mathbf{Y} = \mathbf{X}_{(1)}^T$ ,

$$(\mathbf{H}_3^{-1} \mathbf{A}_2 \otimes \mathbf{I} + \mathbf{H}_3^{-1} \mathbf{M}_1 \otimes \mathbf{M}^{-1} \mathbf{A}_1) \mathbf{Y} + \mathbf{Y} (\mathbf{H}^{-1} \mathbf{A}_3)^T = (\mathbf{H}_3^{-1} \otimes \mathbf{M}^{-1}) \mathbf{B}_{(1)}^T \mathbf{H}^{-T}. \quad (21)$$

Using  $(\mathbf{H}^{-1} \mathbf{A}_3)^T = \mathbf{Q} \mathbf{R} \mathbf{Q}^*$  and multiplying equation (21) on the right by  $\mathbf{Q}$ , we have

$$(\mathbf{H}_3^{-1} \mathbf{A}_2 \otimes \mathbf{I} + \mathbf{H}_3^{-1} \mathbf{M}_1 \otimes \mathbf{M}^{-1} \mathbf{A}_1) \mathbf{Y} \mathbf{Q} + \mathbf{Y} \mathbf{Q} \mathbf{R} = (\mathbf{H}_3^{-1} \otimes \mathbf{M}^{-1}) \mathbf{B}_{(1)}^T \mathbf{H}^{-T} \mathbf{Q}. \quad (22)$$

Let  $\mathbf{Y} \mathbf{Q} =: [\hat{\mathbf{z}}_1, \dots, \hat{\mathbf{z}}_N]$  and  $\mathbf{B}_{(1)}^T \mathbf{H}^{-T} \mathbf{Q} =: [\mathbf{g}_1, \dots, \mathbf{g}_N]$ . Thanks to the upper triangular form of  $\mathbf{R}$ , we have for each  $j = 1, \dots, N$ ,

$$(\mathbf{H}_3^{-1} \mathbf{A}_2 \otimes \mathbf{I} + \mathbf{H}_3^{-1} \mathbf{M}_1 \otimes \mathbf{M}^{-1} \mathbf{A}_1) \hat{\mathbf{z}}_j + \hat{\mathbf{z}}_j R_{j,j} = (\mathbf{H}_3^{-1} \otimes \mathbf{M}^{-1}) \mathbf{g}_j - \mathbf{w}_{j-1}, \quad (23)$$

where we set  $\mathbf{w}_0 = \mathbf{0}$  and  $\mathbf{w}_{j-1} = [\hat{\mathbf{z}}_1, \dots, \hat{\mathbf{z}}_{j-1}] R_{1:j-1, j}$  for  $j = 2, \dots, N$ . Let  $\hat{\mathbf{Z}}_j$ ,  $\mathbf{W}_{j-1}$  and  $\mathbf{G}_j$  be the matrices such that  $\hat{\mathbf{z}}_j = \text{vec}(\hat{\mathbf{Z}}_j)$ ,  $\hat{\mathbf{w}}_{j-1} = \text{vec}(\hat{\mathbf{W}}_{j-1})$  and  $\hat{\mathbf{g}}_j = \text{vec}(\hat{\mathbf{G}}_j)$ . Then, after unvectorizing equation (23), we have

$$\hat{\mathbf{Z}}_j (\mathbf{H}_3^{-1} \mathbf{A}_2)^T + \mathbf{M}^{-1} \mathbf{A}_1 \hat{\mathbf{Z}}_j (\mathbf{H}_3^{-1} \mathbf{M}_1)^T + R_{j,j} \hat{\mathbf{Z}}_j = \mathbf{M}^{-1} \mathbf{G}_j \mathbf{H}_3^{-T} - \mathbf{W}_{j-1}. \quad (24)$$

Rearranging equation (24) and multiplying on the right by  $(\mathbf{H}_3^{-1} \mathbf{M}_1)^{-T}$ , we have

$$\mathbf{M}^{-1} \mathbf{A}_1 \hat{\mathbf{Z}}_j + \hat{\mathbf{Z}}_j (R_{j,j} \mathbf{H}_3^T \mathbf{M}_1^{-T} + \mathbf{A}_2^T \mathbf{M}_1^{-T}) = \mathbf{M}^{-1} \mathbf{G}_j \mathbf{M}_1^{-T} - \mathbf{W}_{j-1} \mathbf{H}_3^T \mathbf{M}_1^{-T}. \quad (25)$$

Solving for  $\hat{\mathbf{Z}}_j$  and computing  $\hat{\mathbf{z}}_j = \text{vec}(\hat{\mathbf{Z}}_j)$ , we get equation (17).

### 3 The implicit RAIL scheme for Tucker tensor solutions

With the preliminaries established, we now introduce the proposed integrator for solving equation (1). The diffusive terms will be evolved implicitly, while the advective terms will be handled explicitly, using implicit-explicit (IMEX) Runge-Kutta time discretizations. As a first step, we describe the implicit RAIL scheme for the diffusion equation, after which we incorporate the advective component. Consider diffusion equations of the form

$$u_t = d_1 u_{xx} + d_2 u_{yy} + d_3 u_{zz}, \quad (26)$$

where  $d_1, d_2, d_3 > 0$  could be time-dependent. Discretizing the solution  $u(x, y, z, t)$  over the tensor product of the uniform computational grids (2), we assume that the numerical solution locally admits a time-dependent low-rank representation as a third-order tensor in the Tucker format,

$$\mathcal{U}(t) = \mathcal{G}(t) \times_1 \mathbf{V}_x(t) \times_2 \mathbf{V}_y(t) \times_3 \mathbf{V}_z(t), \quad (27)$$

where the core tensor, factor matrices (i.e., one-dimensional bases), and multilinear rank  $(r_x(t), r_y(t), r_z(t))$  are time-dependent. Discretizing equation (26) in space sets up the tensor differential equation

$$\begin{aligned} \frac{d}{dt} \left( \mathcal{G}(t) \times_1 \mathbf{V}_x(t) \times_2 \mathbf{V}_y(t) \times_3 \mathbf{V}_z(t) \right) &= \mathcal{G}(t) \times_1 \mathbf{F}_x \mathbf{V}_x(t) \times_2 \mathbf{V}_y(t) \times_3 \mathbf{V}_z(t) \\ &+ \mathcal{G}(t) \times_1 \mathbf{V}_x(t) \times_2 \mathbf{F}_y \mathbf{V}_y(t) \times_3 \mathbf{V}_z(t) \\ &+ \mathcal{G}(t) \times_1 \mathbf{V}_x(t) \times_2 \mathbf{V}_y(t) \times_3 \mathbf{F}_z \mathbf{V}_z(t), \end{aligned} \quad (28)$$

where  $\mathbf{F}_x, \mathbf{F}_y, \mathbf{F}_z$  respectively represent discretizations of the one-dimensional Laplacians  $d_1 \partial_x^2, d_2 \partial_y^2$  and  $d_3 \partial_z^2$ .

#### 3.1 The first-order scheme using implicit Euler discretization

Discretizing the tensor differential equation (28) using implicit Euler method yields the fully discrete tensor equation

$$\begin{aligned} \mathcal{G}^{n+1} \times_1 \mathbf{V}_x^{n+1} \times_2 \mathbf{V}_y^{n+1} \times_3 \mathbf{V}_z^{n+1} &= \mathcal{G}^n \times_1 \mathbf{V}_x^n \times_2 \mathbf{V}_y^n \times_3 \mathbf{V}_z^n \\ &+ \Delta t \left\{ \mathcal{G}^{n+1} \times_1 \mathbf{F}_x \mathbf{V}_x^{n+1} \times_2 \mathbf{V}_y^{n+1} \times_3 \mathbf{V}_z^{n+1} \right. \\ &+ \mathcal{G}^{n+1} \times_1 \mathbf{V}_x^{n+1} \times_2 \mathbf{F}_y \mathbf{V}_y^{n+1} \times_3 \mathbf{V}_z^{n+1} \\ &\left. + \mathcal{G}^{n+1} \times_1 \mathbf{V}_x^{n+1} \times_2 \mathbf{V}_y^{n+1} \times_3 \mathbf{F}_z \mathbf{V}_z^{n+1} \right\}, \end{aligned} \quad (29)$$

where  $\mathcal{U}(t^{n+1}) \approx \mathcal{U}^{n+1} = \mathcal{G}^{n+1} \times_1 \mathbf{V}_x^{n+1} \times_2 \mathbf{V}_y^{n+1} \times_3 \mathbf{V}_z^{n+1}$ . Although we assume constant diffusion coefficients in the following,  $\mathbf{F}_x, \mathbf{F}_y,$  and  $\mathbf{F}_z$  could be time-dependent if the diffusion coefficients vary with time. Following the approach of other low-rank projection-based integrators, we first update the one-dimensional bases by projecting the solution onto subspaces that depend on only one spatial variable at a time. This is followed by a Galerkin projection in all dimensions to update the core tensor.

As such, we update the bases by projecting the solution and equation (29) onto low-dimensional subspaces spanned by some one-dimensional bases  $\mathbf{V}_x^{*,n+1}, \mathbf{V}_y^{*,n+1}$  and  $\mathbf{V}_z^{*,n+1}$ . Since equation (29) uses an implicit time discretization, these bases denoted with a star  $\star$  provide good approximations of the exact bases at time  $t^{n+1}$ , namely,  $\mathbf{V}_x(t^{n+1}), \mathbf{V}_y(t^{n+1})$  and  $\mathbf{V}_z(t^{n+1})$ . For the first-order scheme, we let  $\mathbf{V}_x^{*,n+1} := \mathbf{V}_x^n, \mathbf{V}_y^{*,n+1} := \mathbf{V}_y^n$  and  $\mathbf{V}_z^{*,n+1} := \mathbf{V}_z^n$ . The projected solutions in  $(y, z), (x, z)$  and  $(x, y)$  are then respectively defined by

$$\mathbf{K}_1^{n+1} := \mathbf{V}_x^{n+1} \mathbf{G}_{(1)}^{n+1} ((\mathbf{V}_z^{n+1})^T \mathbf{V}_z^{*,n+1} \otimes (\mathbf{V}_y^{n+1})^T \mathbf{V}_y^{*,n+1}), \quad (30a)$$

$$\mathbf{K}_2^{n+1} := \mathbf{V}_y^{n+1} \mathbf{G}_{(2)}^{n+1} ((\mathbf{V}_z^{n+1})^T \mathbf{V}_z^{*,n+1} \otimes (\mathbf{V}_x^{n+1})^T \mathbf{V}_x^{*,n+1}), \quad (30b)$$

$$\mathbf{K}_3^{n+1} := \mathbf{V}_z^{n+1} \mathbf{G}_{(3)}^{n+1} ((\mathbf{V}_y^{n+1})^T \mathbf{V}_y^{*,n+1} \otimes (\mathbf{V}_x^{n+1})^T \mathbf{V}_x^{*,n+1}), \quad (30c)$$

where each projected solution has been obtained by matricizing it in the respective dimension. Since  $\mathbf{K}_1^{n+1}$  has eliminated the dependence on  $(y, z)$ , it can be used to extract an updated orthonormal basis in  $x$ ; the same applies to  $\mathbf{K}_2^{n+1}$  and  $\mathbf{K}_3^{n+1}$ . Updating these projected solutions is commonly referred to

as the K steps in the literature [6], in particular, the  $K_1$ ,  $K_2$  and  $K_3$  steps. Without loss of generality, we detail only the  $K_1$  step. Performing the mode-1 matricization on equation (29), we have

$$\begin{aligned} \mathbf{V}_x^{n+1} \mathbf{G}_{(1)}^{n+1} (\mathbf{V}_z^{n+1} \otimes \mathbf{V}_y^{n+1})^T &= \mathbf{V}_x^n \mathbf{G}_{(1)}^n (\mathbf{V}_z^n \otimes \mathbf{V}_y^n)^T \\ &+ \Delta t \left\{ \mathbf{F}_x \mathbf{V}_x^{n+1} \mathbf{G}_{(1)}^{n+1} (\mathbf{V}_z^{n+1} \otimes \mathbf{V}_y^{n+1})^T \right. \\ &+ \mathbf{V}_x^{n+1} \mathbf{G}_{(1)}^{n+1} (\mathbf{V}_z^{n+1} \otimes \mathbf{F}_y \mathbf{V}_y^{n+1})^T \\ &\left. + \mathbf{V}_x^{n+1} \mathbf{G}_{(1)}^{n+1} (\mathbf{F}_z \mathbf{V}_z^{n+1} \otimes \mathbf{V}_y^{n+1})^T \right\}. \end{aligned} \quad (31)$$

Projecting equation (31) in  $(y, z)$  using  $\mathbf{V}_y^{*,n+1} = \mathbf{V}_y^n$  and  $\mathbf{V}_z^{*,n+1} = \mathbf{V}_z^n$ , that is, multiplying equation (31) on the right by  $\mathbf{V}_z^n \otimes \mathbf{V}_y^n$ , we have

$$\begin{aligned} \mathbf{V}_x^{n+1} \mathbf{G}_{(1)}^{n+1} ((\mathbf{V}_z^{n+1})^T \mathbf{V}_z^n \otimes (\mathbf{V}_y^{n+1})^T \mathbf{V}_y^n) &= \mathbf{V}_x^n \mathbf{G}_{(1)}^n ((\mathbf{V}_z^n)^T \mathbf{V}_z^n \otimes (\mathbf{V}_y^n)^T \mathbf{V}_y^n) \\ &+ \Delta t \left\{ \mathbf{F}_x \mathbf{V}_x^{n+1} \mathbf{G}_{(1)}^{n+1} ((\mathbf{V}_z^{n+1})^T \mathbf{V}_z^n \otimes (\mathbf{V}_y^{n+1})^T \mathbf{V}_y^n) \right. \\ &+ \mathbf{V}_x^{n+1} \mathbf{G}_{(1)}^{n+1} ((\mathbf{V}_z^{n+1})^T \mathbf{V}_z^n \otimes (\mathbf{F}_y \mathbf{V}_y^{n+1})^T \mathbf{V}_y^n) \\ &\left. + \mathbf{V}_x^{n+1} \mathbf{G}_{(1)}^{n+1} ((\mathbf{F}_z \mathbf{V}_z^{n+1})^T \mathbf{V}_z^n \otimes (\mathbf{V}_y^{n+1})^T \mathbf{V}_y^n) \right\}. \end{aligned} \quad (32)$$

A standard approach to solve equation (32) is to cast it as a Sylvester equation to solve for  $\mathbf{K}_1^{n+1}$ . However, to do so, we must further project the solution in the last two terms of equation (32). Projecting the solution in the appropriate terms in equation (32), we get

$$\mathbf{K}_1^{n+1} = \mathbf{K}_1^n + \Delta t \left\{ \mathbf{F}_x \mathbf{K}_1^{n+1} + \mathbf{K}_1^{n+1} (\mathbf{I}_{r_z^n \times r_z^n} \otimes (\mathbf{F}_y \mathbf{V}_y^n)^T \mathbf{V}_y^n) + \mathbf{K}_1^{n+1} ((\mathbf{F}_z \mathbf{V}_z^n)^T \mathbf{V}_z^n \otimes \mathbf{I}_{r_y^n \times r_y^n}) \right\}, \quad (33)$$

which can be expressed as the Sylvester equation

$$\left( \mathbf{I}_{N_x \times N_x} - \Delta t \mathbf{F}_x \right) \mathbf{K}_1^{n+1} - \mathbf{K}_1^{n+1} \left( \Delta t (\mathbf{F}_z \mathbf{V}_z^n)^T \mathbf{V}_z^n \oplus (\mathbf{F}_y \mathbf{V}_y^n)^T \mathbf{V}_y^n \right) = \mathbf{K}_1^n, \quad (34)$$

where  $\oplus$  denotes the Kronecker sum. We refer to equation (34) as the  $K_1$  equation. Similarly, the  $K_2$  and  $K_3$  equations lead to the Sylvester equations

$$\left( \mathbf{I}_{N_y \times N_y} - \Delta t \mathbf{F}_y \right) \mathbf{K}_2^{n+1} - \mathbf{K}_2^{n+1} \left( \Delta t (\mathbf{F}_z \mathbf{V}_z^n)^T \mathbf{V}_z^n \oplus (\mathbf{F}_x \mathbf{V}_x^n)^T \mathbf{V}_x^n \right) = \mathbf{K}_2^n, \quad (35)$$

$$\left( \mathbf{I}_{N_z \times N_z} - \Delta t \mathbf{F}_z \right) \mathbf{K}_3^{n+1} - \mathbf{K}_3^{n+1} \left( \Delta t (\mathbf{F}_y \mathbf{V}_y^n)^T \mathbf{V}_y^n \oplus (\mathbf{F}_x \mathbf{V}_x^n)^T \mathbf{V}_x^n \right) = \mathbf{K}_3^n. \quad (36)$$

Thus, the K steps reduce to solving three matrix Sylvester equations. Note that the  $K_1$ ,  $K_2$  and  $K_3$  equations can also be solved in parallel, which accelerates computation without impacting the overall computational cost. Referring back to how  $\mathbf{K}_1^{n+1}$  was defined in (30a), the updated orthonormal basis  $\mathbf{V}_x^{n+1}$  can be extracted by a reduced QR factorization,  $\mathbf{K}_1^{n+1} = \mathbf{Q}\mathbf{R} =: \mathbf{V}_x^{\ddagger, n+1} \mathbf{R}$ . We toss the upper triangular matrix  $\mathbf{R}$  since we only need an orthonormal basis. Similarly, we can extract the updated orthonormal bases  $\mathbf{V}_y^{\ddagger, n+1}$  and  $\mathbf{V}_z^{\ddagger, n+1}$  from  $\mathbf{K}_2^{n+1}$  and  $\mathbf{K}_3^{n+1}$ , respectively. Here, the double dagger  $\ddagger$  denotes the one-dimensional orthonormal bases obtained from the K steps that approximate the solution basis at  $t^{n+1}$ .

Following the reduced augmentation procedure from [48], we propose augmenting  $\mathbf{V}_x^{\ddagger, n+1}$  with the previous basis  $\mathbf{V}_x^n$ . Alternatively, we could augment  $\mathbf{V}_x^{\ddagger, n+1}$  with  $\mathbf{K}_1^{n+1}$ , as was proposed in the original augmented BUG integrator [6]. Augmenting the updated and current bases together is advantageous because it ensures that the spanning subspace contains information over the entire time interval  $[t^n, t^{n+1}]$ . This is particularly important when the solution is rapidly evolving, for instance, over short times when solving the diffusion equation.

Unfortunately, in three dimensions this augmentation risks significantly increasing the rank since  $\mathbf{K}_1^{n+1}$  is size  $\sim N \times r^2$ , and so the augmented basis is size  $\sim N \times (r^2 + r)$ . Even for small ranks, this could quickly become costly. To remedy this issue, we reduce (truncate) the augmented basis according to a very small tolerance, usually  $10^{-12}$ . This tolerance is large enough to maintain a low rank, but small enough to not affect the consistency of the scheme. Computing the reduced QR factorizations of the augmented bases,

$$\left[ \mathbf{V}_x^{\ddagger, n+1}, \mathbf{V}_x^n \right] = \mathbf{Q}_x \mathbf{R}_x, \quad \left[ \mathbf{V}_y^{\ddagger, n+1}, \mathbf{V}_y^n \right] = \mathbf{Q}_y \mathbf{R}_y, \quad \left[ \mathbf{V}_z^{\ddagger, n+1}, \mathbf{V}_z^n \right] = \mathbf{Q}_z \mathbf{R}_z. \quad (37)$$

Let  $\hat{r}^{n+1}$  be the maximum of the number of singular values of  $\mathbf{R}_x$ ,  $\mathbf{R}_y$  and  $\mathbf{R}_z$  larger than  $10^{-12}$ ; we also enforce that  $\hat{r}^{n+1}$  be no larger than the lengths of  $\mathbf{R}_x$ ,  $\mathbf{R}_y$  and  $\mathbf{R}_z$ . We then let the reduced augmented basis  $\hat{\mathbf{V}}_x^{n+1}$  be  $\mathbf{Q}_x$  multiplied on the right by the first  $\hat{r}^{n+1}$  left singular vectors of  $\mathbf{R}_x$ , and similarly to obtain  $\hat{\mathbf{V}}_y^{n+1}$  and  $\hat{\mathbf{V}}_z^{n+1}$ . With that, we can now perform a Galerkin projection onto the subspace generated by these (reduced) updated one-dimensional bases to update the core tensor  $\hat{\mathcal{G}}^{n+1}$ . This Galerkin projection is called the G step, analogous to the S step in the DLR/BUG literature for solving two-dimensional problems. Here, we have used hats to denote the factorized solution produced by the K<sub>1</sub>-K<sub>2</sub>-K<sub>3</sub>-G procedure. Vectorizing equation (29), we have

$$\begin{aligned} (\mathbf{V}_z^{n+1} \otimes \mathbf{V}_y^{n+1} \otimes \mathbf{V}_x^{n+1}) \text{vec}(\mathcal{G}^{n+1}) &= (\mathbf{V}_z^n \otimes \mathbf{V}_y^n \otimes \mathbf{V}_x^n) \text{vec}(\mathcal{G}^n) \\ &\quad + \Delta t \left\{ (\mathbf{V}_z^{n+1} \otimes \mathbf{V}_y^{n+1} \otimes \mathbf{F}_x \mathbf{V}_x^{n+1}) \text{vec}(\mathcal{G}^{n+1}) \right. \\ &\quad + (\mathbf{V}_z^{n+1} \otimes \mathbf{F}_y \mathbf{V}_y^{n+1} \otimes \mathbf{V}_x^{n+1}) \text{vec}(\mathcal{G}^{n+1}) \\ &\quad \left. + (\mathbf{F}_z \mathbf{V}_z^{n+1} \otimes \mathbf{V}_y^{n+1} \otimes \mathbf{V}_x^{n+1}) \text{vec}(\mathcal{G}^{n+1}) \right\}. \end{aligned} \quad (38)$$

Performing a Galerkin projection onto the updated bases obtained via reduced augmentation,

$$\text{vec}(\hat{\mathcal{G}}^{n+1}) := ((\hat{\mathbf{V}}_z^{n+1})^T \mathbf{V}_z^{n+1} \otimes (\hat{\mathbf{V}}_y^{n+1})^T \mathbf{V}_y^{n+1} \otimes (\hat{\mathbf{V}}_x^{n+1})^T \mathbf{V}_x^{n+1}) \text{vec}(\mathcal{G}^{n+1}). \quad (39)$$

Similar to the K steps, we project equation (38) onto the updated bases by multiplying on the left by  $(\hat{\mathbf{V}}_z^{n+1} \otimes \hat{\mathbf{V}}_y^{n+1} \otimes \hat{\mathbf{V}}_x^{n+1})^T$  to get the third order tensor linear equation

$$\begin{aligned} &\left\{ \left( \mathbf{I}_{\hat{r}^{n+1} \times \hat{r}^{n+1}} - \Delta t (\hat{\mathbf{V}}_z^{n+1})^T (\mathbf{F}_z \hat{\mathbf{V}}_z^{n+1}) \right) \otimes \mathbf{I}_{\hat{r}^{n+1} \times \hat{r}^{n+1}} \otimes \mathbf{I}_{\hat{r}^{n+1} \times \hat{r}^{n+1}} \right. \\ &\quad + \mathbf{I}_{\hat{r}^{n+1} \times \hat{r}^{n+1}} \otimes \left( -\Delta t (\hat{\mathbf{V}}_y^{n+1})^T (\mathbf{F}_y \hat{\mathbf{V}}_y^{n+1}) \right) \otimes \mathbf{I}_{\hat{r}^{n+1} \times \hat{r}^{n+1}} \\ &\quad \left. + \mathbf{I}_{\hat{r}^{n+1} \times \hat{r}^{n+1}} \otimes \mathbf{I}_{\hat{r}^{n+1} \times \hat{r}^{n+1}} \otimes \left( -\Delta t (\hat{\mathbf{V}}_x^{n+1})^T (\mathbf{F}_x \hat{\mathbf{V}}_x^{n+1}) \right) \right\} \text{vec}(\hat{\mathcal{G}}^{n+1}) = \text{vec}(\hat{\mathcal{G}}^n). \end{aligned} \quad (40)$$

Observe that all the coefficient matrices are the same size since the reduced augmentation procedure kept  $\hat{r}^{n+1}$  singular values for all spatial dimensions. This was intentionally done so that the solver in Corollary 1, extended from the solver in [58], could be used to efficiently compute  $\mathcal{G}^{n+1}$ . After using the method described in Corollary 1 to solve for  $\mathcal{G}^{n+1}$ , we truncate the Tucker tensor solution by using the multilinear SVD (MLSVD) [10], also known as the higher order SVD (HOSVD), to compress the core tensor. We use the `mlsvd` function in the MATLAB toolbox Tensorlab [63, 64] to compress  $\hat{\mathcal{G}}^{n+1}$  according to tolerance  $\varepsilon$ , usually between  $10^{-5}$  and  $10^{-8}$ ; we acknowledge KU Leuven as the provider of the software. The result is a (small) Tucker tensor of multilinear rank  $(r_x^{n+1}, r_y^{n+1}, r_z^{n+1})$  that approximates the core tensor,

$$\hat{\mathcal{G}}^{n+1} \approx \mathcal{G}^{n+1} \times_1 \mathbf{G}_x^{n+1} \times_2 \mathbf{G}_y^{n+1} \times_3 \mathbf{G}_z^{n+1}, \quad (41)$$

where  $\mathbf{G}_x^{n+1}$ ,  $\mathbf{G}_y^{n+1}$  and  $\mathbf{G}_z^{n+1}$  have orthonormal column vectors, and  $\mathcal{G}^{n+1}$  is defined to be the final updated core tensor. The final updated one-dimensional bases/factor matrices of the Tucker tensor solution are then  $\mathbf{V}_x^{n+1} = \hat{\mathbf{V}}_x^{n+1} \mathbf{G}_x^{n+1}$ ,  $\mathbf{V}_y^{n+1} = \hat{\mathbf{V}}_y^{n+1} \mathbf{G}_y^{n+1}$  and  $\mathbf{V}_z^{n+1} = \hat{\mathbf{V}}_z^{n+1} \mathbf{G}_z^{n+1}$ .

### 3.2 Higher-order schemes using diagonally implicit Runge-Kutta (DIRK) discretizations

We extend the implicit RAIL scheme to high-order accuracy by evolving equation (28) using diagonally implicit Runge-Kutta (DIRK) methods [29]. A general  $s$  stage DIRK method is typically expressed in a Butcher tableau given by Table 1,

Table 1: Butcher tableau for an  $s$  stage DIRK scheme

$c_1$	$a_{11}$	0	...	0
$c_2$	$a_{21}$	$a_{22}$	...	0
$\vdots$	$\vdots$	$\vdots$	$\ddots$	$\vdots$
$c_s$	$a_{s1}$	$a_{s2}$	...	$a_{ss}$
	$b_1$	$b_2$	...	$b_s$

where  $c_k = \sum_{j=1}^k a_{kj}$  for  $k = 1, 2, \dots, s$ , and  $\sum_{k=1}^s b_k = 1$  for consistency. Each row in the Butcher tableau represents an intermediate stage for the solution at time  $t^{(k)} = t^n + c_k \Delta t$  for  $1, 2, \dots, s$ . In particular, the intermediate equation at the  $k$ th stage is

$$\begin{aligned} \mathcal{G}^{(k)} \times_1 \mathbf{V}_x^{(k)} \times_2 \mathbf{V}_y^{(k)} \times_3 \mathbf{V}_z^{(k)} &= \mathcal{G}^n \times_1 \mathbf{V}_x^n \times_2 \mathbf{V}_y^n \times_3 \mathbf{V}_z^n \\ &+ \Delta t \sum_{\ell=1}^k a_{k\ell} \left\{ \mathcal{G}^{(\ell)} \times_1 \mathbf{F}_x \mathbf{V}_x^{(\ell)} \times_2 \mathbf{V}_y^{(\ell)} \times_3 \mathbf{V}_z^{(\ell)} \right. \\ &\quad + \mathcal{G}^{(\ell)} \times_1 \mathbf{V}_x^{(\ell)} \times_2 \mathbf{F}_y \mathbf{V}_y^{(\ell)} \times_3 \mathbf{V}_z^{(\ell)} \\ &\quad \left. + \mathcal{G}^{(\ell)} \times_1 \mathbf{V}_x^{(\ell)} \times_2 \mathbf{V}_y^{(\ell)} \times_3 \mathbf{F}_z \mathbf{V}_z^{(\ell)} \right\}, \end{aligned} \quad (42)$$

where  $\mathcal{G}^{(k)} \times_1 \mathbf{V}_x^{(k)} \times_2 \mathbf{V}_y^{(k)} \times_3 \mathbf{V}_z^{(k)} = \mathcal{U}^{(k)} \approx \mathcal{U}(t^{(k)})$ . With the intermediate stages computed for  $k = 1, 2, \dots, s$ , the final solution is

$$\begin{aligned} \mathcal{G}^{n+1} \times_1 \mathbf{V}_x^{n+1} \times_2 \mathbf{V}_y^{n+1} \times_3 \mathbf{V}_z^{n+1} &= \mathcal{G}^n \times_1 \mathbf{V}_x^n \times_2 \mathbf{V}_y^n \times_3 \mathbf{V}_z^n \\ &+ \Delta t \sum_{k=1}^s b_k \left\{ \mathcal{G}^{(k)} \times_1 \mathbf{F}_x \mathbf{V}_x^{(k)} \times_2 \mathbf{V}_y^{(k)} \times_3 \mathbf{V}_z^{(k)} \right. \\ &\quad + \mathcal{G}^{(k)} \times_1 \mathbf{V}_x^{(k)} \times_2 \mathbf{F}_y \mathbf{V}_y^{(k)} \times_3 \mathbf{V}_z^{(k)} \\ &\quad \left. + \mathcal{G}^{(k)} \times_1 \mathbf{V}_x^{(k)} \times_2 \mathbf{V}_y^{(k)} \times_3 \mathbf{F}_z \mathbf{V}_z^{(k)} \right\}. \end{aligned} \quad (43)$$

We restrict ourselves to stiffly accurate DIRK methods for which  $c_s = 1$  and  $a_{sk} = b_k$  for  $k = 1, 2, \dots, s$ . As such,  $\mathcal{U}^{(s)} = \mathcal{U}^{n+1}$  and we do not need to compute equation (43). The high-order RAIL scheme performs the K<sub>1</sub>-K<sub>2</sub>-K<sub>3</sub>-G (and truncate) procedure using enriched projection subspaces defined by  $\mathbf{V}_*^{x,(k)}$ ,  $\mathbf{V}_*^{y,(k)}$  and  $\mathbf{V}_*^{z,(k)}$  at each subsequent stage. The question that remains is: how do we define the approximate bases  $\mathbf{V}_*^{x,(k)}$ ,  $\mathbf{V}_*^{y,(k)}$  and  $\mathbf{V}_*^{z,(k)}$  at each stage? Since the RAIL framework discretizes in time before performing the project, we have the flexibility to construct richer low-rank subspaces at *each RK stage* using the bases computed at the previous stages.

**K<sub>1</sub>-K<sub>2</sub>-K<sub>3</sub> Steps.** The first-order scheme only used the reduced augmentation procedure preceding the G step, see equation (37). For the high-order scheme, we will use the reduced augmentation procedure before the K<sub>1</sub>-K<sub>2</sub>-K<sub>3</sub> steps (to construct the approximate bases) *and* before the G step. Without loss of generality of the dimension, at the  $k$ -th RK stage, we reduce the augmented basis

$$\left[ \mathbf{V}_x^{\dagger,(k)}, \mathbf{V}_x^{(k-1)}, \dots, \mathbf{V}_x^{(1)}, \mathbf{V}_x^{(0)} \right], \quad (44)$$

where  $\mathbf{V}_x^{(0)} = \mathbf{V}_x^n$ , and  $\mathbf{V}_x^{\dagger,(k)}$  denotes a first-order prediction at time  $t^{(k)}$  computed using the first-order RAIL scheme. Similar to equation (37), a first-order prediction at the future time  $t^{(k)}$  is included in the augmented basis so that the subspace contains information over the entire time interval  $[t^n, t^{(k)}]$ . Note that  $\mathbf{V}_x^{\dagger,(k)}$  is only needed for  $k > 1$  since the first stage  $k = 1$  is itself a backward Euler discretization. After computing the reduced QR factorizations of the augmented bases, the projection bases  $\mathbf{V}_x^{*,(k)}$ ,  $\mathbf{V}_y^{*,(k)}$ ,  $\mathbf{V}_z^{*,(k)}$  are constructed in the same manner as in the first-order scheme, where the singular values of the upper triangular factors  $\mathbf{R}_x$ ,  $\mathbf{R}_y$ ,  $\mathbf{R}_z$  are truncated according to a small tolerance  $10^{-12}$ . We summarize the *reduced augmentation procedure* in Algorithm 1.

The projected solutions in  $(y, z)$ ,  $(x, z)$  and  $(x, y)$  are respectively defined by (30a), (30b) and (30c); naturally, a superscript  $(k)$  can be used to denote the projected solutions at time  $t^{(k)}$ . Following the same detailed procedure outlined in subsection 3.1 for the K<sub>1</sub> step, but instead working with equation (42), one obtains the Sylvester equation

$$\left( \mathbf{I}_{N_x \times N_x} - a_{kk} \Delta t \mathbf{F}_x \right) \mathbf{K}_1^{(k)} - \mathbf{K}_1^{(k)} \left( a_{kk} \Delta t (\mathbf{F}_z \mathbf{V}_z^{*,(k)})^T \mathbf{V}_z^{*,(k)} \oplus (\mathbf{F}_y \mathbf{V}_y^{*,(k)})^T \mathbf{V}_y^{*,(k)} \right) = \mathbf{W}_1^{(k-1)}, \quad (45)$$

where

$$\begin{aligned}
\mathbf{W}_1^{(k-1)} &= \mathbf{V}_x^n \mathbf{G}_{(1)}^n ((\mathbf{V}_z^n)^T \mathbf{V}_z^{*,(k)} \otimes (\mathbf{V}_y^n)^T \mathbf{V}_y^{*,(k)}) \\
&+ \Delta t \sum_{\ell=1}^{k-1} a_{k\ell} \left\{ (\mathbf{F}_x \mathbf{V}_x^{(\ell)}) \mathbf{G}_{(1)}^{(\ell)} ((\mathbf{V}_z^{(\ell)})^T \mathbf{V}_z^{*,(k)} \otimes (\mathbf{V}_y^{(\ell)})^T \mathbf{V}_y^{*,(k)}) \right. \\
&\quad + \mathbf{V}_x^{(\ell)} \mathbf{G}_{(1)}^{(\ell)} ((\mathbf{V}_z^{(\ell)})^T \mathbf{V}_z^{*,(k)} \otimes (\mathbf{F}_y \mathbf{V}_y^{(\ell)})^T \mathbf{V}_y^{*,(k)}) \\
&\quad \left. + \mathbf{V}_x^{(\ell)} \mathbf{G}_{(1)}^{(\ell)} ((\mathbf{F}_z \mathbf{V}_z^{(\ell)})^T \mathbf{V}_z^{*,(k)} \otimes (\mathbf{V}_y^{(\ell)})^T \mathbf{V}_y^{*,(k)}) \right\}. \tag{46}
\end{aligned}$$

The  $\mathbf{K}_2$  and  $\mathbf{K}_3$  Sylvester equations can be derived similarly. With  $\mathbf{K}_1^{(k)}$ ,  $\mathbf{K}_2^{(k)}$  and  $\mathbf{K}_3^{(k)}$  computed, a reduced QR factorization extracts orthonormal bases for each dimension. That is,  $\mathbf{K}_1^{(k)} = \mathbf{QR} =: \mathbf{V}_x^{\ddagger,(k)} \mathbf{R}$ , and similarly for  $\mathbf{V}_y^{\ddagger,(k)}$  and  $\mathbf{V}_z^{\ddagger,(k)}$ . As with the first-order scheme, a double dagger  $\ddagger$  denotes the one-dimensional orthonormal bases obtained from the K steps that approximate the solution basis at  $t^{(k)}$ .

G Step. Replacing  $\mathbf{V}^{\dagger,(k)}$  with  $\mathbf{V}^{\ddagger,(k)}$  in the augmented matrices, e.g., equation (44) for  $x$ -dimension, we perform the reduced augmentation procedure to obtain the pre-truncated bases  $\hat{\mathbf{V}}^{(k)}$ . We again let hats denote the factorized solution produced by the  $\mathbf{K}_1$ - $\mathbf{K}_2$ - $\mathbf{K}_3$ -G procedure. Performing a Galerkin projection onto these updated bases,

$$\text{vec}(\hat{\mathcal{G}}^{(k)}) := ((\hat{\mathbf{V}}_z^{(k)})^T \mathbf{V}_z^{(k)} \otimes (\hat{\mathbf{V}}_y^{(k)})^T \mathbf{V}_y^{(k)} \otimes (\hat{\mathbf{V}}_x^{(k)})^T \mathbf{V}_x^{(k)}) \text{vec}(\mathcal{G}^{(k)}). \tag{47}$$

Vectorizing equation (42) and projecting onto the updated bases  $\hat{\mathbf{V}}^{(k)}$ , we get the third-order tensor linear equation

$$\begin{aligned}
&\left\{ \left( \mathbf{I}_{\hat{r}^{(k)} \times \hat{r}^{(k)}} - a_{kk} \Delta t (\hat{\mathbf{V}}_z^{(k)})^T (\mathbf{F}_z \hat{\mathbf{V}}_z^{(k)}) \right) \otimes \mathbf{I}_{\hat{r}^{(k)} \times \hat{r}^{(k)}} \otimes \mathbf{I}_{\hat{r}^{(k)} \times \hat{r}^{(k)}} \right. \\
&\quad + \mathbf{I}_{\hat{r}^{(k)} \times \hat{r}^{(k)}} \otimes \left( -a_{kk} \Delta t (\hat{\mathbf{V}}_y^{(k)})^T (\mathbf{F}_y \hat{\mathbf{V}}_y^{(k)}) \right) \otimes \mathbf{I}_{\hat{r}^{(k)} \times \hat{r}^{(k)}} \\
&\quad \left. + \mathbf{I}_{\hat{r}^{(k)} \times \hat{r}^{(k)}} \otimes \mathbf{I}_{\hat{r}^{(k)} \times \hat{r}^{(k)}} \otimes \left( -a_{kk} \Delta t (\hat{\mathbf{V}}_x^{(k)})^T (\mathbf{F}_x \hat{\mathbf{V}}_x^{(k)}) \right) \right\} \text{vec}(\hat{\mathcal{G}}^{(k)}) = \text{vec}(\mathcal{B}^{(k-1)}), \tag{48}
\end{aligned}$$

where

$$\begin{aligned}
\mathcal{B}^{(k-1)} &= \mathcal{G}^n \times_1 (\hat{\mathbf{V}}_x^{(k)})^T \mathbf{V}_x^n \times_2 (\hat{\mathbf{V}}_y^{(k)})^T \mathbf{V}_y^n \times_3 (\hat{\mathbf{V}}_z^{(k)})^T \mathbf{V}_z^n \\
&+ \Delta t \sum_{\ell=1}^{k-1} a_{k\ell} \left\{ \mathcal{G}^{(\ell)} \times_1 (\hat{\mathbf{V}}_x^{(k)})^T (\mathbf{F}_x \mathbf{V}_x^{(\ell)}) \times_2 (\hat{\mathbf{V}}_y^{(k)})^T \mathbf{V}_y^{(\ell)} \times_3 (\hat{\mathbf{V}}_z^{(k)})^T \mathbf{V}_z^{(\ell)} \right. \\
&\quad + \mathcal{G}^{(\ell)} \times_1 (\hat{\mathbf{V}}_x^{(k)})^T \mathbf{V}_x^{(\ell)} \times_2 (\hat{\mathbf{V}}_y^{(k)})^T (\mathbf{F}_y \mathbf{V}_y^{(\ell)}) \times_3 (\hat{\mathbf{V}}_z^{(k)})^T \mathbf{V}_z^{(\ell)} \\
&\quad \left. + \mathcal{G}^{(\ell)} \times_1 (\hat{\mathbf{V}}_x^{(k)})^T \mathbf{V}_x^{(\ell)} \times_2 (\hat{\mathbf{V}}_y^{(k)})^T \mathbf{V}_y^{(\ell)} \times_3 (\hat{\mathbf{V}}_z^{(k)})^T (\mathbf{F}_z \mathbf{V}_z^{(\ell)}) \right\}. \tag{49}
\end{aligned}$$

The direct solver described in Corollary 1 is used to solve equation (48) for  $\hat{\mathcal{G}}^{(k)}$ . According to some tolerance  $\varepsilon$ , usually between  $10^{-5}$  and  $10^{-8}$ , the HOSVD is then used to approximate the core tensor by a compressed Tucker tensor of multilinear rank  $(r_x^{(k)}, r_y^{(k)}, r_z^{(k)})$ ,

$$\hat{\mathcal{G}}^{(k)} \approx \mathcal{G}^{(k)} \times_1 \mathbf{G}_x^{(k)} \times_2 \mathbf{G}_y^{(k)} \times_3 \mathbf{G}_z^{(k)}. \tag{50}$$

Thus, the final updated solution at stage  $k$  is described by the core tensor  $\mathcal{G}^{(k)}$ , and the one-dimensional bases/factor matrices  $\mathbf{V}_x^{(k)} = \hat{\mathbf{V}}_x^{(k)} \mathbf{G}_x^{(k)}$ ,  $\mathbf{V}_y^{(k)} = \hat{\mathbf{V}}_y^{(k)} \mathbf{G}_y^{(k)}$  and  $\mathbf{V}_z^{(k)} = \hat{\mathbf{V}}_z^{(k)} \mathbf{G}_z^{(k)}$ . Repeating this process for each subsequent stage in the stiffly accurate DIRK method, we eventually obtain the final updated solution  $\mathcal{U}^{n+1} = \mathcal{U}^{(s)} = \mathcal{G}^{(s)} \times_1 \mathbf{V}_x^{(s)} \times_2 \mathbf{V}_y^{(s)} \times_3 \mathbf{V}_z^{(s)}$ .

### 3.3 Consistency and stability analysis of the implicit scheme

An important quality of DLR-type methods is the availability of consistency and stability analysis, which ensures their reliability in practical applications. These properties have been well-established in lower-dimensional settings, offering a solid theoretical foundation for numerical approximations. The RAIL-2D algorithm in [48] proves consistency and stability for the first-order implicit scheme, and discusses the intuition behind the numerically observed high-order consistency. In this work, we extend these results to the proposed 3D setting, where the added complexity of high-dimensional tensors necessitates a careful tensorial formulation. To maintain clarity, we first focus on the first-order implicit RAIL-3D scheme for the diffusion equation, which serves as a natural starting point for analyzing the behavior of the implicit RAIL approach. We then include a remark on the high-order consistency without rigorous derivation, although high-order accuracy is observed in all numerical experiments conducted in this paper.

The consistency of the first-order scheme follows naturally, as it coincides with the BUG integrator for Tucker tensors proposed in [6], where an implicit Euler numerical scheme is applied to the intermediate sub-steps for  $K_1$ - $K_2$ - $K_3$ - $G$ . We thus recall, for completeness of exposition, the consistency result from [6]. We state the theorem an informal level and omit the proof.

**Theorem 3 ([6])** *Let the right-hand side of (28) be Lipschitz continuous and uniformly bounded, with  $L$  being the Lipschitz constant and  $B$  being the uniform bound. Furthermore, assume that in a neighborhood of the exact solution, the right-hand side remains within  $\sigma$ -distance from its projection onto the tangent space of the rank- $r$  low-rank manifold. Let  $\mathcal{U}^1$  the approximation obtained from the first-order implicit RAIL-3D algorithm after a single time-step  $\Delta t > 0$ . Supposing that  $\mathcal{U}^0$  is the exact initial condition, we obtain that*

$$\|\mathcal{U}(t^1) - \mathcal{U}^1\|_F \leq \Delta t(c_1\sigma + c_2\Delta t) + c_3\varepsilon, \quad (51)$$

where the constants  $c_i$  only depend on  $L$ ,  $B$ , and a bound on  $\Delta t$ . Here,  $\varepsilon$  denotes the tolerance with which we compress the core tensor in the truncated HOSVD.

Although we only presented a local error bound to keep the focus on the scheme's consistency, Ceruti et al. [6] also rigorously proved convergence (a global error bound) for the first-order implicit BUG integrator for Tucker tensors. The same convergence theorem also holds for our proposed first-order implicit RAIL-3D scheme. We note that unlike the BUG integrator, the RAIL formulation reduces the augmented basis with respect to a very small tolerance of  $10^{-12}$ . Formally, this reduction adds another term to the above local error bound on the order of  $10^{-12}$ . However, since roundoff errors are not taken into account in the original theorem, this reduction will effectively not change the consistency (or convergence) of the scheme.

While consistency ensures that the scheme approximates the continuous problem correctly as the discretization parameters tend to zero, stability is crucial to guarantee that numerical errors do not grow uncontrollably over time. The following theorem addresses the stability properties of the first-order implicit RAIL-3D scheme, ensuring controlled error growth under suitable assumptions.

**Theorem 4** *Assuming  $\mathbf{F}_x$ ,  $\mathbf{F}_y$ , and  $\mathbf{F}_z$  are symmetric and negative semi-definite, the first-order backward RAIL scheme before truncation is unconditionally stable, that is,*

$$\|\hat{\mathcal{G}}^{n+1}\|_F \leq \|\hat{\mathcal{G}}^n\|_F.$$

*Proof* The proof extends the result originally provided in Theorem 2 of [48] from the matrix setting to the tensorial setting. For clarity, matrix dimensions are omitted in the following. To simplify the notation, we introduce the symmetric matrices:

$$\begin{aligned} \mathbf{A} &:= \Delta t(\hat{\mathbf{V}}_z^{n+1})^T(\mathbf{F}_z\hat{\mathbf{V}}_z^{n+1}), \\ \mathbf{B} &:= \Delta t(\hat{\mathbf{V}}_y^{n+1})^T(\mathbf{F}_y\hat{\mathbf{V}}_y^{n+1}), \\ \mathbf{C} &:= \Delta t(\hat{\mathbf{V}}_x^{n+1})^T(\mathbf{F}_x\hat{\mathbf{V}}_x^{n+1}). \end{aligned}$$

The update of  $\hat{\mathcal{G}}^{n+1}$  can be concisely expressed as the following tensor equation:

$$\hat{\mathcal{G}}^{n+1} \times_1 (\mathbf{I} - \mathbf{A}) - \hat{\mathcal{G}}^{n+1} \times_2 \mathbf{B} - \hat{\mathcal{G}}^{n+1} \times_3 \mathbf{C} = \hat{\mathcal{G}}^n.$$

Unfolding the above equation along the first mode, we obtain:

$$(\mathbf{I} - \mathbf{A})\hat{\mathbf{G}}^{n+1} - \hat{\mathbf{G}}^{n+1}(\mathbf{I} \otimes \mathbf{B}) - \hat{\mathbf{G}}^{n+1}(\mathbf{C} \otimes \mathbf{I}) = \hat{\mathbf{G}}^n.$$

where the matrices  $\hat{\mathbf{G}}^{n+1}$  and  $\hat{\mathbf{G}}^n$  represent the matricization of the tensors  $\hat{\mathcal{G}}^{n+1}$  and  $\hat{\mathcal{G}}^n$  along the first mode, respectively. For simplicity, we omit the subscript indicating the matricization mode. Now, we diagonalize the matrices  $\mathbf{A}$ ,  $\mathbf{B}$ , and  $\mathbf{C}$ , which are symmetric and semi-definite; thus, they admit diagonal representations such as

$$\begin{aligned}\mathbf{D} &:= \mathbf{P}^T \mathbf{A} \mathbf{P}, \\ \mathbf{E} &:= \mathbf{Q}^T \mathbf{B} \mathbf{Q}, \\ \mathbf{F} &:= \mathbf{R}^T \mathbf{C} \mathbf{R},\end{aligned}$$

where the factors  $\mathbf{P}$ ,  $\mathbf{Q}$ , and  $\mathbf{R}$  are orthonormal, e.g.  $\mathbf{P}\mathbf{P}^T = \mathbf{P}^T\mathbf{P} = \mathbf{I}$ . Moreover, we have that

$$(\mathbf{Q} \otimes \mathbf{R})(\mathbf{Q}^T \otimes \mathbf{R}^T) = \mathbf{I} \otimes \mathbf{I}.$$

We continue by diagonalizing the matrices appearing in the matrix equation. We begin by multiplying from the right with  $\mathbf{P}^T$  and  $(\mathbf{Q} \otimes \mathbf{R})$  on the left. This yields the intermediate matrix equation:

$$\mathbf{P}^T(\mathbf{I} - \mathbf{A})\hat{\mathbf{G}}^{n+1}(\mathbf{Q} \otimes \mathbf{R}) - \mathbf{P}^T\hat{\mathbf{G}}^{n+1}(\mathbf{I} \otimes \mathbf{B} + \mathbf{C} \otimes \mathbf{I})(\mathbf{Q} \otimes \mathbf{R}) = \mathbf{P}^T\hat{\mathbf{G}}^n(\mathbf{Q} \otimes \mathbf{R}).$$

If we introduce the auxiliary variables

$$\tilde{\mathbf{G}}^{n+1} := \mathbf{P}^T\hat{\mathbf{G}}^{n+1}(\mathbf{Q} \otimes \mathbf{R}), \quad \tilde{\mathbf{G}}^n := \mathbf{P}^T\hat{\mathbf{G}}^n(\mathbf{Q} \otimes \mathbf{R}),$$

the matrix equation simplifies to

$$\mathbf{P}^T(\mathbf{I} - \mathbf{A})\mathbf{P}\tilde{\mathbf{G}}^{n+1} - \tilde{\mathbf{G}}^{n+1}(\mathbf{Q}^T \otimes \mathbf{R}^T)(\mathbf{I} \otimes \mathbf{B} + \mathbf{C} \otimes \mathbf{I})(\mathbf{Q} \otimes \mathbf{R}) = \tilde{\mathbf{G}}^n.$$

Thus, since most of the factors in the expression above can be diagonalized, we obtain

$$(\mathbf{I} - \mathbf{D})\tilde{\mathbf{G}}^{n+1} - \tilde{\mathbf{G}}^{n+1}(\mathbf{I} \otimes \mathbf{E} + \mathbf{F} \otimes \mathbf{I}) = \tilde{\mathbf{G}}^n.$$

It follows that

$$\tilde{G}_{ij}^{n+1} = \alpha_{ij}\tilde{G}_{ij}^n, \quad \text{with} \quad \alpha_{ij} = \frac{1}{1 - D_{ii} - E_{jj} - F_{jj}}.$$

Since the eigenvalues are strictly negative, the amplification factor  $\alpha_{ij}$  is less than or equal to 1. Thus,

$$\|\hat{\mathcal{G}}^{n+1}\|_{\mathbf{F}} = \|\hat{\mathbf{G}}^{n+1}\|_{\mathbf{F}} = \|\tilde{\mathbf{G}}^{n+1}\|_{\mathbf{F}} \leq \|\tilde{\mathbf{G}}^n\|_{\mathbf{F}},$$

The conclusion follows by recalling that, analogously,  $\|\tilde{\mathbf{G}}^n\|_{\mathbf{F}} = \|\hat{\mathcal{G}}^n\|_{\mathbf{F}}$ .

*Remark 2* Rigorously deriving a robust local error bound for the high-order RAIL scheme is highly nontrivial, especially due to the implicit time-stepping. Only recently has significant progress been made by others in proving higher than first-order accuracy for BUG-type methods using explicit time-stepping methods. We suffice to comment on the intuition behind why and when we expect a high-order error bound to exist, and we only verify high-order accuracy in our numerical tests conducted here.

The reduced augmentation procedure includes the bases computed at all the previous RK stages. In doing so, we generate a projection subspace as large and rich as possible to allow for the high-order accuracy obtained in the final stage of the RK method to be observed in the numerical experiments. However, as stated in Theorem 3 [6], the first-order algorithm requires the right-hand side (e.g., the Laplacian of the solution) to remain close to the tangent space. Naturally, we expect similar assumptions to be needed for our high-order extension. We also reiterate that the purpose of including a first-order approximation in the augmentation at each RK stage is to include a prediction of the updated basis (because of using implicit time discretizations). Whereas, the bases from the previous RK stages are included to generate a rich space so that the consistency order of the RK method can still be observed.

#### 4 The implicit-explicit RAIL scheme for Tucker tensor solutions

We now incorporate the advection and source terms in equation (1). In order to express equation (1) as a tensor differential equation, we must first discretize the linear advection and source terms in space. Moreover, the advection and source terms need to be expressed as low-multilinear rank Tucker tensors in order to fit our projection based procedure and maintain computational efficiency. Consider the advection term

$$(a_1(\mathbf{x}, t)u)_x + (a_2(\mathbf{x}, t)u)_y + (a_3(\mathbf{x}, t)u)_z, \quad (52)$$

where the flow field  $\mathbf{a}(\mathbf{x}, t) = a_1(\mathbf{x}, t)\hat{x} + a_2(\mathbf{x}, t)\hat{y} + a_3(\mathbf{x}, t)\hat{z}$  is assumed low-rank. Under this assumption, the scalar flow field in each direction can be expressed as a low-multilinear rank Tucker tensor. That is, for  $i = 1, 2, 3$ , the function  $a_i(\mathbf{x}, t)$  can be discretized as a time-dependent Tucker tensor,

$$\mathcal{A}_i(t) = \mathcal{G}_i^a(t) \times_1 \mathbf{A}_{i,x}(t) \times_2 \mathbf{A}_{i,y}(t) \times_3 \mathbf{A}_{i,z}(t). \quad (53)$$

For  $i = 1, 2, 3$ , we require a Tucker decomposition that stores the flux function  $a_i(\mathbf{x}, t)u(\mathbf{x}, t)$  over the tensorized computational grid. Since  $a_i(\mathbf{x}, t)$  and  $u(\mathbf{x}, t)$  are each stored in Tucker tensors, we need the Tucker decomposition of the Hadamard product of two Tucker tensors, namely  $\mathcal{E}_i(t) = \mathcal{A}_i(t) * \mathcal{U}(t)$ . By Theorem 2,

$$\mathcal{E}_i(t) = \mathcal{G}_i^e \times_1 \mathbf{E}_{i,x} \times_2 \mathbf{E}_{i,y} \times_3 \mathbf{E}_{i,z} := (\mathcal{G}_i^a \otimes \mathcal{U}) \times_1 (\mathbf{A}_{i,x} \odot^T \mathbf{V}_x) \times_2 (\mathbf{A}_{i,y} \odot^T \mathbf{V}_y) \times_3 (\mathbf{A}_{i,z} \odot^T \mathbf{V}_z). \quad (54)$$

Further assume the source term  $q(\mathbf{x}, t)$  can be stored as a low-multilinear rank Tucker tensor  $\mathcal{G}(t) = \mathcal{G}^c(t) \times_1 \mathbf{C}_x(t) \times_2 \mathbf{C}_y(t) \times_3 \mathbf{C}_z(t)$ . Discretizing equation (1) in space sets up the tensor differential equation

$$\begin{aligned} \frac{d}{dt} \left( \mathcal{G}(t) \times_1 \mathbf{V}_x(t) \times_2 \mathbf{V}_y(t) \times_3 \mathbf{V}_z(t) \right) &= \left\{ \mathcal{G}(t) \times_1 \mathbf{F}_x \mathbf{V}_x(t) \times_2 \mathbf{V}_y(t) \times_3 \mathbf{V}_z(t) \right. \\ &\quad + \mathcal{G}(t) \times_1 \mathbf{V}_x(t) \times_2 \mathbf{F}_y \mathbf{V}_y(t) \times_3 \mathbf{V}_z(t) \\ &\quad \left. + \mathcal{G}(t) \times_1 \mathbf{V}_x(t) \times_2 \mathbf{V}_y(t) \times_3 \mathbf{F}_z \mathbf{V}_z(t) \right\} \\ &- \left\{ \mathcal{G}_1^e(t) \times_1 \mathbf{D}_x \mathbf{E}_{1,x}(t) \times_2 \mathbf{E}_{1,y}(t) \times_3 \mathbf{E}_{1,z}(t) \right. \\ &\quad + \mathcal{G}_2^e(t) \times_1 \mathbf{E}_{2,x}(t) \times_2 \mathbf{D}_y \mathbf{E}_{2,y}(t) \times_3 \mathbf{E}_{2,z}(t) \\ &\quad \left. + \mathcal{G}_3^e(t) \times_1 \mathbf{E}_{3,x}(t) \times_2 \mathbf{E}_{3,y}(t) \times_3 \mathbf{D}_z \mathbf{E}_{3,z}(t) \right\} \\ &+ \mathcal{G}^c(t) \times_1 \mathbf{C}_x(t) \times_2 \mathbf{C}_y(t) \times_3 \mathbf{C}_z(t), \end{aligned} \quad (55)$$

where  $\mathbf{D}_x, \mathbf{D}_y, \mathbf{D}_z$  respectively discretize the one-dimensional partial derivatives  $\partial_x, \partial_y, \partial_z$ .

##### 4.1 The first-order scheme using implicit Euler-backward Euler discretization

Discretizing the tensor differential equation (55) using implicit Euler-backward Euler method yields the fully discrete tensor equation

$$\begin{aligned} \mathcal{G}^{n+1} \times_1 \mathbf{V}_x^{n+1} \times_2 \mathbf{V}_y^{n+1} \times_3 \mathbf{V}_z^{n+1} &= \mathcal{G}^n \times_1 \mathbf{V}_x^n \times_2 \mathbf{V}_y^n \times_3 \mathbf{V}_z^n \\ &+ \Delta t \left\{ \mathcal{G}^{n+1} \times_1 \mathbf{F}_x \mathbf{V}_x^{n+1} \times_2 \mathbf{V}_y^{n+1} \times_3 \mathbf{V}_z^{n+1} \right. \\ &\quad + \mathcal{G}^{n+1} \times_1 \mathbf{V}_x^{n+1} \times_2 \mathbf{F}_y \mathbf{V}_y^{n+1} \times_3 \mathbf{V}_z^{n+1} \\ &\quad \left. + \mathcal{G}^{n+1} \times_1 \mathbf{V}_x^{n+1} \times_2 \mathbf{V}_y^{n+1} \times_3 \mathbf{F}_z \mathbf{V}_z^{n+1} \right\} \\ &- \Delta t \left\{ \mathcal{G}_1^{e,n} \times_1 \mathbf{D}_x \mathbf{E}_{1,x}^n \times_2 \mathbf{E}_{1,y}^n \times_3 \mathbf{E}_{1,z}^n \right. \\ &\quad + \mathcal{G}_2^{e,n} \times_1 \mathbf{E}_{2,x}^n \times_2 \mathbf{D}_y \mathbf{E}_{2,y}^n \times_3 \mathbf{E}_{2,z}^n \\ &\quad \left. + \mathcal{G}_3^{e,n} \times_1 \mathbf{E}_{3,x}^n \times_2 \mathbf{E}_{3,y}^n \times_3 \mathbf{D}_z \mathbf{E}_{3,z}^n \right\} \\ &+ \Delta t \left\{ \mathcal{G}^{c,n+1} \times_1 \mathbf{C}_x^{n+1} \times_2 \mathbf{C}_y^{n+1} \times_3 \mathbf{C}_z^{n+1} \right\}, \end{aligned} \quad (56)$$

where the diffusion and source terms are evolved implicitly using backward Euler discretization, and the advection terms are evolved explicitly using forward Euler discretization; the source term could also be evolved explicitly if needed.

Table 2: Implicit RK Scheme

0	0	0	0	0	0
$c_1$	0	$a_{11}$	0	...	0
$c_2$	0	$a_{21}$	$a_{22}$	...	0
$\vdots$	$\vdots$	$\vdots$	$\vdots$	$\ddots$	$\vdots$
$c_s$	0	$a_{s1}$	$a_{s2}$	...	$a_{ss}$
	0	$b_1$	$b_2$	...	$b_s$

Table 3: Explicit RK Scheme

0	0	0	0	...	0
$c_1$	$\tilde{a}_{21}$	0	0	...	0
$c_2$	$\tilde{a}_{31}$	$\tilde{a}_{32}$	0	...	0
$\vdots$	$\vdots$	$\vdots$	$\vdots$	$\ddots$	$\vdots$
$c_s$	$\tilde{a}_{\sigma 1}$	$\tilde{a}_{\sigma 2}$	$\tilde{a}_{\sigma 3}$	...	0
	$b_1$	$b_2$	$b_3$	...	$b_\sigma$

The first-order implicit-explicit (IMEX) RAIL scheme follows identically to the first-order implicit RAIL scheme in subsection 3.1 with the only exception being the righthand sides of the K and G equations now also include the previous advection terms and the (known) source term. We suffice to just write the  $K_1$  and G equations here; the  $K_2$  and  $K_3$  equations can be easily derived following subsection 3.1. The  $K_1$  equation is

$$\left(\mathbf{I}_{N_x \times N_x} - \Delta t \mathbf{F}_x\right) \mathbf{K}_1^{n+1} - \mathbf{K}_1^{n+1} \left(\Delta t (\mathbf{F}_z \mathbf{V}_z^n)^T \mathbf{V}_z^n \oplus (\mathbf{F}_y \mathbf{V}_y^n)^T \mathbf{V}_y^n\right) = \mathbf{W}_1^n, \quad (57)$$

where

$$\begin{aligned} \mathbf{W}_1^n = & \mathbf{K}_1^n - \Delta t \left\{ (\mathbf{D}_x \mathbf{E}_{1,x}^n) \mathbf{G}_{1,(1)}^{e,n} \left( (\mathbf{E}_{1,z}^n)^T \mathbf{V}_z^n \otimes (\mathbf{E}_{1,y}^n)^T \mathbf{V}_y^n \right) \right. \\ & + \mathbf{E}_{2,x}^n \mathbf{G}_{2,(1)}^{e,n} \left( (\mathbf{E}_{2,z}^n)^T \mathbf{V}_z^n \otimes (\mathbf{D}_y \mathbf{E}_{2,y}^n)^T \mathbf{V}_y^n \right) \\ & + \mathbf{E}_{3,x}^n \mathbf{G}_{3,(1)}^{e,n} \left( (\mathbf{D}_z \mathbf{E}_{3,z}^n)^T \mathbf{V}_z^n \otimes (\mathbf{E}_{3,y}^n)^T \mathbf{V}_y^n \right) \left. \right\} \\ & + \Delta t \left\{ \mathbf{C}_x^{n+1} \mathbf{G}_{(1)}^{c,n+1} \left( (\mathbf{C}_z^{n+1})^T \mathbf{V}_z^n \otimes (\mathbf{C}_y^{n+1})^T \mathbf{V}_y^n \right) \right\}. \end{aligned} \quad (58)$$

The G equation is

$$\begin{aligned} & \left\{ \left( \mathbf{I}_{\hat{r}^{n+1} \times \hat{r}^{n+1}} - \Delta t (\hat{\mathbf{V}}_z^{n+1})^T (\mathbf{F}_z \hat{\mathbf{V}}_z^{n+1}) \right) \otimes \mathbf{I}_{\hat{r}^{n+1} \times \hat{r}^{n+1}} \otimes \mathbf{I}_{\hat{r}^{n+1} \times \hat{r}^{n+1}} \right. \\ & + \mathbf{I}_{\hat{r}^{n+1} \times \hat{r}^{n+1}} \otimes \left( - \Delta t (\hat{\mathbf{V}}_y^{n+1})^T (\mathbf{F}_y \hat{\mathbf{V}}_y^{n+1}) \right) \otimes \mathbf{I}_{\hat{r}^{n+1} \times \hat{r}^{n+1}} \\ & \left. + \mathbf{I}_{\hat{r}^{n+1} \times \hat{r}^{n+1}} \otimes \mathbf{I}_{\hat{r}^{n+1} \times \hat{r}^{n+1}} \otimes \left( - \Delta t (\hat{\mathbf{V}}_x^{n+1})^T (\mathbf{F}_x \hat{\mathbf{V}}_x^{n+1}) \right) \right\} \text{vec}(\mathcal{G}^{n+1}) = \text{vec}(\mathcal{B}^n), \end{aligned} \quad (59)$$

where

$$\begin{aligned} \mathcal{B}^n = & \mathcal{G}^n \times_1 (\hat{\mathbf{V}}_x^{n+1})^T \mathbf{V}_x^n \times_2 (\hat{\mathbf{V}}_y^{n+1})^T \mathbf{V}_y^n \times_3 (\hat{\mathbf{V}}_z^{n+1})^T \mathbf{V}_z^n \\ & - \Delta t \left\{ \mathcal{G}_1^{e,n} \times_1 (\hat{\mathbf{V}}_x^{n+1})^T (\mathbf{D}_x \mathbf{E}_{1,x}^n) \times_2 (\hat{\mathbf{V}}_y^{n+1})^T \mathbf{E}_{1,y}^n \times_3 (\hat{\mathbf{V}}_z^{n+1})^T \mathbf{E}_{1,z}^n \right. \\ & + \mathcal{G}_2^{e,n} \times_1 (\hat{\mathbf{V}}_x^{n+1})^T \mathbf{E}_{2,x}^n \times_2 (\hat{\mathbf{V}}_y^{n+1})^T (\mathbf{D}_y \mathbf{E}_{2,y}^n) \times_3 (\hat{\mathbf{V}}_z^{n+1})^T \mathbf{E}_{2,z}^n \\ & + \mathcal{G}_3^{e,n} \times_1 (\hat{\mathbf{V}}_x^{n+1})^T \mathbf{E}_{3,x}^n \times_2 (\hat{\mathbf{V}}_y^{n+1})^T \mathbf{E}_{3,y}^n \times_3 (\hat{\mathbf{V}}_z^{n+1})^T (\mathbf{D}_z \mathbf{E}_{3,z}^n) \left. \right\} \\ & + \Delta t \left\{ \mathcal{G}^{c,n+1} \times_1 (\hat{\mathbf{V}}_x^{n+1})^T \mathbf{C}_x^{n+1} \times_2 (\hat{\mathbf{V}}_y^{n+1})^T \mathbf{C}_y^{n+1} \times_3 (\hat{\mathbf{V}}_z^{n+1})^T \mathbf{C}_z^{n+1} \right\}. \end{aligned} \quad (60)$$

#### 4.2 Higher-order schemes using implicit-explicit (IMEX) Runge-Kutta discretizations

We extend the RAIL scheme to higher-order using the IMEX RK methods from [2]. Following the notation from [2],  $\text{IMEX}(s, \sigma, p)$  couples an  $s$  stage DIRK scheme with a  $\sigma = s + 1$  stage explicit RK scheme, with combined order  $p$ .  $\text{IMEX}(s, \sigma, p)$  RK methods are expressed by two Butcher tableaus, one each for the implicit and explicit RK methods, as seen in Tables 2 and 3. In particular, we use IMEX RK methods that incorporate stiffly accurate DIRK methods for the implicit treatment. As such,  $\mathcal{U}^{n+1} = \mathcal{U}^{(s)}$  and we only need to compute the solution at the intermediate stages. Discretizing the tensor differential

equation (55) in time, the equation for the intermediate solution  $\mathcal{U}^{(k)} \approx \mathcal{U}(t^{(k)} = t^n + c_k \Delta t)$  at the  $k$ th stage is (for  $k = 1, 2, \dots, s$ )

$$\begin{aligned}
\mathcal{G}^{(k)} \times_1 \mathbf{V}_x^{(k)} \times_2 \mathbf{V}_y^{(k)} \times_3 \mathbf{V}_z^{(k)} &= \mathcal{G}^n \times_1 \mathbf{V}_x^n \times_2 \mathbf{V}_y^n \times_3 \mathbf{V}_z^n \\
&+ \Delta t \sum_{\ell=1}^k a_{k\ell} \left\{ \mathcal{G}^{(\ell)} \times_1 \mathbf{F}_x \mathbf{V}_x^{(\ell)} \times_2 \mathbf{V}_y^{(\ell)} \times_3 \mathbf{V}_z^{(\ell)} \right. \\
&\quad + \mathcal{G}^{(\ell)} \times_1 \mathbf{V}_x^{(\ell)} \times_2 \mathbf{F}_y \mathbf{V}_y^{(\ell)} \times_3 \mathbf{V}_z^{(\ell)} \\
&\quad \left. + \mathcal{G}^{(\ell)} \times_1 \mathbf{V}_x^{(\ell)} \times_2 \mathbf{V}_y^{(\ell)} \times_3 \mathbf{F}_z \mathbf{V}_z^{(\ell)} \right\} \\
&- \Delta t \sum_{\ell=1}^k \tilde{a}_{k+1,\ell} \left\{ \mathcal{G}_1^{e,(\ell-1)} \times_1 \mathbf{D}_x \mathbf{E}_{1,x}^{(\ell-1)} \times_2 \mathbf{E}_{1,y}^{(\ell-1)} \times_3 \mathbf{E}_{1,z}^{(\ell-1)} \right. \\
&\quad + \mathcal{G}_2^{e,(\ell-1)} \times_1 \mathbf{E}_{2,x}^{(\ell-1)} \times_2 \mathbf{D}_y \mathbf{E}_{2,y}^{(\ell-1)} \times_3 \mathbf{E}_{2,z}^{(\ell-1)} \\
&\quad \left. + \mathcal{G}_3^{e,(\ell-1)} \times_1 \mathbf{E}_{3,x}^{(\ell-1)} \times_2 \mathbf{E}_{3,y}^{(\ell-1)} \times_3 \mathbf{D}_z \mathbf{E}_{3,z}^{(\ell-1)} \right\} \\
&+ \Delta t \sum_{\ell=1}^k a_{k\ell} \left\{ \mathcal{G}^{c,(\ell)} \times_1 \mathbf{C}_x^{(\ell)} \times_2 \mathbf{C}_y^{(\ell)} \times_3 \mathbf{C}_z^{(\ell)} \right\}.
\end{aligned} \tag{61}$$

The high-order IMEX RAIL scheme follows identically to the high-order implicit RAIL scheme in subsection 3.2 with two small modifications: (1) the righthand sides of the K and G equations at the  $k$ th stage now also include the known advection terms from the previous stages and the source terms from the first  $k$  stages, and (2) the first-order predictions  $\mathbf{V}_x^{\dagger,(k)}$ ,  $\mathbf{V}_y^{\dagger,(k)}$  and  $\mathbf{V}_z^{\dagger,(k)}$  in the reduced augmentation for the K<sub>1</sub>-K<sub>2</sub>-K<sub>3</sub> steps (see equation (44)) are computed using the first-order IMEX RAIL scheme from subsection 4.1. The high-order IMEX RAIL scheme for equation (1) is outlined in Algorithm 2. We suffice to just write the K<sub>1</sub> and G equations for the  $k$ th stage here; the K<sub>2</sub> and K<sub>3</sub> equations can be easily derived by following the procedures from the previous sections. The K<sub>1</sub> equation is the same as equation (45) but with

$$\begin{aligned}
\mathbf{W}_1^{(k-1)} &= \mathbf{V}_x^n \mathbf{G}_{(1)}^n ((\mathbf{V}_z^n)^T \mathbf{V}_z^{*,(k)} \otimes (\mathbf{V}_y^n)^T \mathbf{V}_y^{*,(k)}) \\
&+ \Delta t \sum_{\ell=1}^{k-1} a_{k\ell} \left\{ (\mathbf{F}_x \mathbf{V}_x^{(\ell)}) \mathbf{G}_{(1)}^{(\ell)} ((\mathbf{V}_z^{(\ell)})^T \mathbf{V}_z^{*,(k)} \otimes (\mathbf{V}_y^{(\ell)})^T \mathbf{V}_y^{*,(k)}) \right. \\
&\quad + \mathbf{V}_x^{(\ell)} \mathbf{G}_{(1)}^{(\ell)} ((\mathbf{V}_z^{(\ell)})^T \mathbf{V}_z^{*,(k)} \otimes (\mathbf{F}_y \mathbf{V}_y^{(\ell)})^T \mathbf{V}_y^{*,(k)}) \\
&\quad \left. + \mathbf{V}_x^{(\ell)} \mathbf{G}_{(1)}^{(\ell)} ((\mathbf{F}_z \mathbf{V}_z^{(\ell)})^T \mathbf{V}_z^{*,(k)} \otimes (\mathbf{V}_y^{(\ell)})^T \mathbf{V}_y^{*,(k)}) \right\} \\
&- \Delta t \sum_{\ell=1}^k \tilde{a}_{k+1,\ell} \left\{ (\mathbf{D}_x \mathbf{E}_{1,x}^{(\ell-1)}) \mathbf{G}_{1,(1)}^{e,(\ell-1)} ((\mathbf{E}_{1,z}^{(\ell-1)})^T \mathbf{V}_z^{*,(k)} \otimes (\mathbf{E}_{1,y}^{(\ell-1)})^T \mathbf{V}_y^{*,(k)}) \right. \\
&\quad + \mathbf{E}_{2,x}^{(\ell-1)} \mathbf{G}_{2,(1)}^{e,(\ell-1)} ((\mathbf{E}_{2,z}^{(\ell-1)})^T \mathbf{V}_z^{*,(k)} \otimes (\mathbf{D}_y \mathbf{E}_{2,y}^{(\ell-1)})^T \mathbf{V}_y^{*,(k)}) \\
&\quad \left. + \mathbf{E}_{3,x}^{(\ell-1)} \mathbf{G}_{3,(1)}^{e,(\ell-1)} ((\mathbf{D}_z \mathbf{E}_{3,z}^{(\ell-1)})^T \mathbf{V}_z^{*,(k)} \otimes (\mathbf{E}_{3,y}^{(\ell-1)})^T \mathbf{V}_y^{*,(k)}) \right\} \\
&+ \Delta t \sum_{\ell=1}^k a_{k\ell} \left\{ \mathbf{C}_x^{(\ell)} \mathbf{G}_{(1)}^{c,(\ell)} ((\mathbf{C}_z^{(\ell)})^T \mathbf{V}_z^{*,(k)} \otimes (\mathbf{C}_y^{(\ell)})^T \mathbf{V}_y^{*,(k)}) \right\}.
\end{aligned} \tag{62}$$

The G equation is the same as equation (48) but with

$$\begin{aligned}
\mathcal{B}^{(k-1)} &= \mathcal{G}^n \times_1 (\hat{\mathbf{V}}_x^{(k)})^T \mathbf{V}_x^n \times_2 (\hat{\mathbf{V}}_y^{(k)})^T \mathbf{V}_y^n \times_3 (\hat{\mathbf{V}}_z^{(k)})^T \mathbf{V}_z^n \\
&+ \Delta t \sum_{\ell=1}^{k-1} a_{k\ell} \left\{ \mathcal{G}^{(\ell)} \times_1 (\hat{\mathbf{V}}_x^{(k)})^T (\mathbf{F}_x \mathbf{V}_x^{(\ell)}) \times_2 (\hat{\mathbf{V}}_y^{(k)})^T \mathbf{V}_y^{(\ell)} \times_3 (\hat{\mathbf{V}}_z^{(k)})^T \mathbf{V}_z^{(\ell)} \right. \\
&\quad + \mathcal{G}^{(\ell)} \times_1 (\hat{\mathbf{V}}_x^{(k)})^T \mathbf{V}_x^{(\ell)} \times_2 (\hat{\mathbf{V}}_y^{(k)})^T (\mathbf{F}_y \mathbf{V}_y^{(\ell)}) \times_3 (\hat{\mathbf{V}}_z^{(k)})^T \mathbf{V}_z^{(\ell)} \\
&\quad \left. + \mathcal{G}^{(\ell)} \times_1 (\hat{\mathbf{V}}_x^{(k)})^T \mathbf{V}_x^{(\ell)} \times_2 (\hat{\mathbf{V}}_y^{(k)})^T \mathbf{V}_y^{(\ell)} \times_3 (\hat{\mathbf{V}}_z^{(k)})^T (\mathbf{F}_z \mathbf{V}_z^{(\ell)}) \right\} \\
&- \Delta t \sum_{\ell=1}^k \tilde{a}_{k+1,\ell} \left\{ \mathcal{G}_1^{e,(\ell-1)} \times_1 (\hat{\mathbf{V}}_x^{(k)})^T (\mathbf{D}_x \mathbf{E}_{1,x}^{(\ell-1)}) \times_2 (\hat{\mathbf{V}}_y^{(k)})^T \mathbf{E}_{1,y}^{(\ell-1)} \times_3 (\hat{\mathbf{V}}_z^{(k)})^T \mathbf{E}_{1,z}^{(\ell-1)} \right. \\
&\quad + \mathcal{G}_2^{e,(\ell-1)} \times_1 (\hat{\mathbf{V}}_x^{(k)})^T \mathbf{E}_{2,x}^{(\ell-1)} \times_2 (\hat{\mathbf{V}}_y^{(k)})^T (\mathbf{D}_y \mathbf{E}_{2,y}^{(\ell-1)}) \times_3 (\hat{\mathbf{V}}_z^{(k)})^T \mathbf{E}_{2,z}^{(\ell-1)} \\
&\quad \left. + \mathcal{G}_3^{e,(\ell-1)} \times_1 (\hat{\mathbf{V}}_x^{(k)})^T \mathbf{E}_{3,x}^{(\ell-1)} \times_2 (\hat{\mathbf{V}}_y^{(k)})^T \mathbf{E}_{3,y}^{(\ell-1)} \times_3 (\hat{\mathbf{V}}_z^{(k)})^T (\mathbf{D}_z \mathbf{E}_{3,z}^{(\ell-1)}) \right\} \\
&+ \Delta t \left\{ \mathcal{G}^{c,(\ell)} \times_1 (\hat{\mathbf{V}}_x^{(k)})^T \mathbf{C}_x^{(\ell)} \times_2 (\hat{\mathbf{V}}_y^{(k)})^T \mathbf{C}_y^{(\ell)} \times_3 (\hat{\mathbf{V}}_z^{(k)})^T \mathbf{C}_z^{(\ell)} \right\}.
\end{aligned} \tag{63}$$

#### 4.3 Computational complexity

We briefly comment on the computational complexity of the RAIL-3D algorithm. The proposed algorithm offers an efficient way to solve three-dimensional diffusion and advection-diffusion equations that exhibit low-rank solutions. However, we highlight the steps in the algorithm that will observe increased computational complexity if the rank  $r$  starts increasing. Depending on how low-rank the solution is, the computational cost of each time-step is dominated by the reduced augmentation, the K steps, and/or the G step due to the direct solver for the third-order tensor linear equation.

Each augmented matrix (44) that needs to be reduced is size  $N \times r(k+1)$ , where  $k = 1, 2, \dots, s$  is the stage of the RK method. As such, computing a reduced QR factorization will cost  $\sim N^2 r(s+1)$  flops for the last RK stage. Hence, the computational cost of the reduced augmentations will increase with higher-order RK methods as more stages are required.

The dominant computational cost of the K steps comes from solving matrix Sylvester equations. Without loss of generality, the coefficient matrices involved in the  $K_1$  equation are  $\mathbf{I} - a_{kk} \Delta t \mathbf{F}_x$  of size  $N \times N$  and  $a_{kk} \Delta t (\mathbf{F}_z \mathbf{V}_z^{*,(k)})^T \mathbf{V}_z^{*,(k)} \oplus (\mathbf{F}_y \mathbf{V}_y^{*,(k)})^T \mathbf{V}_y^{*,(k)}$  of size  $r^2 \times r^2$ . As such, most standard Sylvester solvers, e.g., [3, 24], will have a computational cost dominated by  $\sim N^3$  flops, assuming  $r \ll N$ . However, if the rank  $r$  starts significantly increasing, the other flop counts on the order of  $\sim N^2 r^2$ ,  $\sim N r^4$  and  $\sim r^6$  will noticeably affect the computational cost.

Similarly, the direct solver used in the G step boils down to solving several Sylvester equations (18). Since we use the direct solver to solve the G equation (48) in which all the coefficient matrices are of size  $r \times r$ , the computational cost for solving each Sylvester equation will be dominated by  $\sim r^3$  flops. Doing this  $r$  times for the direct solver will result in the G step costing  $\sim r^4$  flops.

We also note that when solving advection-diffusion equations, the rank of the flow field can increase the cost. As seen in equation (54), we require the Tucker decomposition of the Hadamard product of two Tucker tensors: the scalar flow field and the solution. However, the core tensor of the resulting Tucker decomposition is the Kronecker product of two third-order core tensors. Assuming the (multilinear) rank of the flow field is  $r'$  and the (multilinear) rank of the solution is  $r$ , the size of the resulting core tensor is  $rr' \times rr' \times rr'$ . As a result, the computational cost of subsequent steps greatly increases if the rank of the flow field is relatively large. In the numerical tests considered in this paper, we assume extremely low-rank flow fields. If more general low-rank flow fields are considered, then further compression techniques might be needed for the resulting Tucker decomposition in order to maintain efficiency; see [35].

## 5 Numerical experiments

We now demonstrate the efficiency and verify the accuracy of the proposed RAIL algorithm by testing it on various benchmark problems. Rank plots show how well the scheme captures low-rank solution structures, and  $L^1$  error plots demonstrate the high-order accuracy in time. We assume a uniform mesh

in space with  $N = N_x = N_y = N_z$  gridpoints in each dimension. Given the uniform mesh, spectral collocation methods discretize the one-dimensional spatial derivatives, with the differentiation matrices found in [60]. As such, we expect the temporal error to dominate. Although we assume periodic boundary conditions, other boundary conditions (and hence other differentiation matrices) could be used. For solutions that decay at infinity (e.g., Gaussian distribution functions), the computational domain is made large enough for sufficient smoothness at the boundary for spectral methods to be used assuming periodic boundary conditions.

As in the two-dimensional RAIL scheme [48], the time-stepping size for the three-dimensional RAIL scheme appears to satisfy a CFL condition when using IMEX discretizations due to the explicit RK method used to evolve the non-stiff terms. It has been shown, at least in the discontinuous Galerkin framework, that when solving advection-diffusion problems with IMEX discretizations, the time-stepping size must be upper-bounded by a constant dependent on the ratio of the diffusion and the square of the advection coefficients [65]. Although our proposed scheme is in the finite difference framework, we observed similar restrictions in our numerical tests. As such, when solving advection-diffusion equations with flow fields  $\mathbf{a}(\mathbf{x}, t) = a_1(\mathbf{x}, t)\hat{x} + a_2(\mathbf{x}, t)\hat{y} + a_3(\mathbf{x}, t)\hat{z}$  in our numerical tests, we define the time-stepping size by

$$\Delta t = \frac{\lambda}{\frac{\max |a_1|}{\Delta x} + \frac{\max |a_2|}{\Delta y} + \frac{\max |a_3|}{\Delta z}}, \quad (64)$$

where  $\lambda > 0$  is the CFL scaling factor. We define the  $L^1$  error as

$$\|u - u_{\text{exact}}\|_1 := \Delta x \Delta y \Delta z \sum_{i=1}^{N_x} \sum_{j=1}^{N_y} \sum_{k=1}^{N_z} |u_{ijk} - u_{\text{exact},ijk}|, \quad (65)$$

where we do not scale by measure of the domain. Lastly, we set the low-rank tolerance  $\varepsilon$  between  $10^{-6}$  and  $10^{-8}$ . In practice, this tolerance can be made larger than  $10^{-6}$ , although we want to ensure it is smaller than the local truncation error.

### Example 1 (Diffusion equation)

$$u_t = d_1 u_{xx} + d_2 u_{yy} + d_3 u_{zz}, \quad x, y, z \in (0, 14) \quad (66)$$

with anisotropic diffusion coefficients  $d_1 = 1/3$ ,  $d_2 = 1/4$  and  $d_3 = 1/5$ . We consider a rank-two initial condition consisting of two Gaussian distributions,

$$u(\mathbf{x}, t = 0) = 0.8 \exp(-15|\mathbf{x} - 6.5|^2) + 0.5 \exp(-15|\mathbf{x} - 7.5|^2). \quad (67)$$

Since we evolve diffusion equations only with implicit time discretizations, we define the time-stepping size as

$$\Delta t = \frac{\lambda}{\frac{1}{\Delta x} + \frac{1}{\Delta y} + \frac{1}{\Delta z}}. \quad (68)$$

As seen in Figure 2, the expected accuracies are observed for the implicit RAIL scheme when using backward Euler, DIRK2 and DIRK3. We used a mesh size  $N = 100$ , tolerance  $\varepsilon = 10^{-6}$ , final time  $T_f = 0.5$ , and  $\lambda$  ranging from 0.5 to 3. A reference solution was computed using a mesh size  $N = 100$ , tolerance  $\varepsilon = 10^{-13}$ ,  $\lambda = 0.01$ , and DIRK3 for the time discretization.

The multilinear rank  $(r_1, r_2, r_3)$  and the average of the multilinear rank  $(r_1 + r_2 + r_3)/3$  of the solution are shown in Figure 4 for backward Euler, DIRK2 and DIRK3. For the rank plots, we used a mesh size  $N = 100$ , final time  $T_f = 5$ , tolerance  $\varepsilon = 10^{-6}$ , and  $\lambda = 0.5$ . Due to the diffusive dynamics, we expect the rank-two initial condition (67) to instantaneously increase in rank and then rapidly decrease as the solution approaches equilibrium. All three time discretizations capture this rank behavior, with higher-order schemes better capturing the rank decay towards equilibrium.

### Example 2 (Advection-diffusion with constant coefficients)

$$u_t + u_x + u_y + u_z = d(u_{xx} + u_{yy} + u_{zz}), \quad x, y, z \in (-\pi, \pi) \quad (69)$$

where  $d = 1/6$ . We use the first two Fourier modes as the initial condition, with the exact solution

$$u(x, y, z, t) = \sum_{k=1}^2 e^{-3dk^2 t} \sin(k(x-t)) \sin(k(y-t)) \sin(k(z-t)). \quad (70)$$

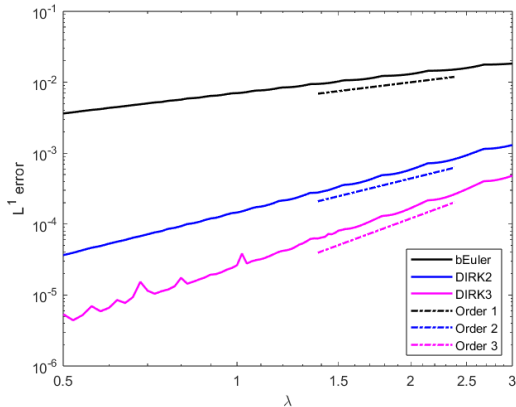


Fig. 2: Error plot for (66) with initial condition (67) using backward Euler, DIRK2 and DIRK3.

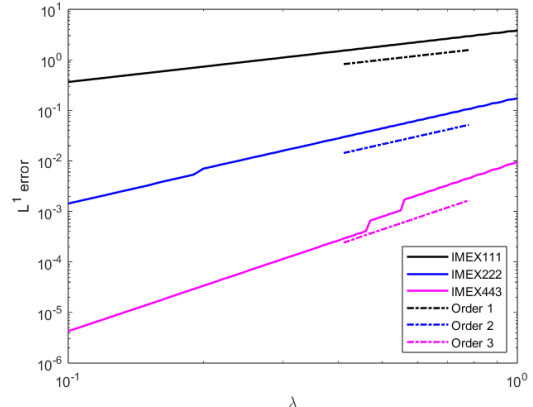


Fig. 3: Error plot for (69) with initial condition  $u_0(x, y, z, ) = \sum_{k=1}^2 \sin(kx) \sin(ky) \sin(kz)$  using IMEX111, IMEX222 and IMEX443.

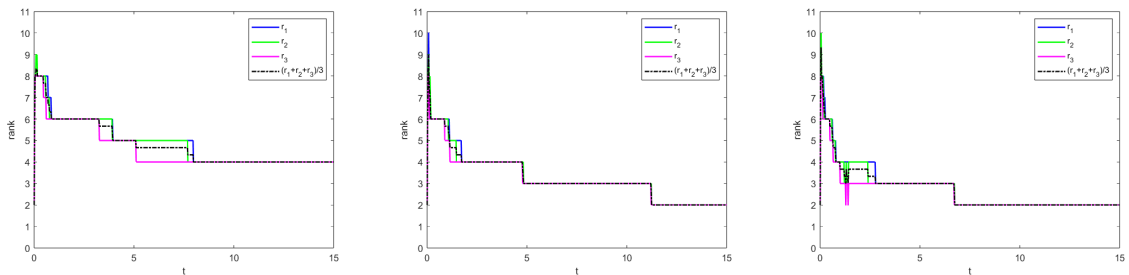


Fig. 4: The multilinear rank  $(r_1, r_2, r_3)$  and average of the multilinear rank  $(r_1 + r_2 + r_3)/3$  of the solution to (66) with initial condition (67) using backward Euler (*left*), DIRK2 (*middle*) and DIRK3 (*right*).

As seen in Figure 3, the expected accuracies are observed for the RAIL scheme when using IMEX111, IMEX222 and IMEX443. We used a mesh size  $N = 80$ , tolerance  $\varepsilon = 10^{-6}$ , final time  $T_f = 0.3$ , and  $\lambda$  ranging from 0.1 to 1. Despite observing the expected accuracy, the  $L^1$  error for the first-order scheme (and even the second-order scheme) is quite large. However, recall that we do not scale the  $L^1$  error by the measure of the domain, which in this case would be  $|\Omega| = (2\pi)^3$ ; scaling by the measure of the domain would provide a better comparison against the  $L^\infty$  error which is not as large.

### Example 3 (Rigid body rotation with diffusion, about $\hat{z}$ )

$$u_t - yu_x + xu_y = d(u_{xx} + u_{yy} + u_{zz}) + c(x, y, z, t), \quad x, y, z \in (-2\pi, 2\pi) \quad (71)$$

where the flow field describes rotation about the vector  $\hat{z}$ . To test the accuracy of the scheme, we use the manufactured solution  $u(x, y, z, t) = \exp(-(x^2 + 2y^2 + 3z^2 + 3dt))$  with  $d = 1/3$ , for which the source term  $c(x, y, z, t)$  offsets the rotation and is

$$c(x, y, z, t) = e^{-(x^2 + 2y^2 + 3z^2 + 3dt)} \left( -2xy - d(-9 + 4x^2 + 16y^2 + 36z^2) \right). \quad (72)$$

As seen in Figure 5, the expected accuracies are observed for the RAIL scheme when using IMEX111, IMEX222 and IMEX443. We used a mesh size  $N = 80$ , tolerance  $\varepsilon = 10^{-8}$ , final time  $T_f = 0.3$ , and  $\lambda$  ranging from 0.5 to 2. When a low-rank source term is involved, we must express it in a Tucker tensor format. By inspection, it is straightforward for one to write down a Tucker decomposition of (72).

To test the rank of the solution, we set  $d = 1/12$ ,  $c(x, y, z, t) = 0$ , double the speed of the rotation,

$$u_t - 2yu_x + 2xu_y = \frac{1}{12}(u_{xx} + u_{yy} + u_{zz}), \quad x, y, z \in (-2\pi, 2\pi) \quad (73)$$

and set the initial condition to  $u_0(x, y, z) = \exp(-(x^2 + 9y^2 + z^2))$ . The solution rotates counterclockwise about the positive  $z$ -axis while slowly diffusing. Theoretically, the exact multilinear rank should be

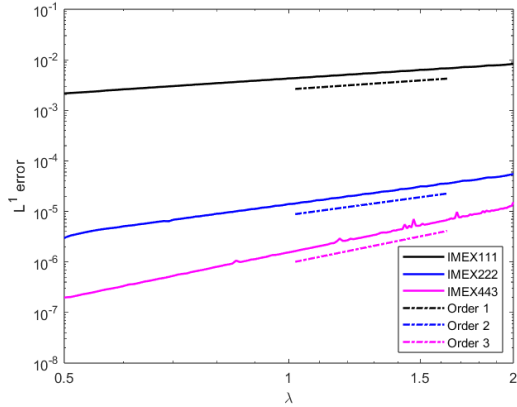


Fig. 5: Error plot for (71) with initial condition  $u_0(x, y, z) = \exp(-(x^2 + 2y^2 + 3z^2))$  using IMEX111, IMEX222 and IMEX443.

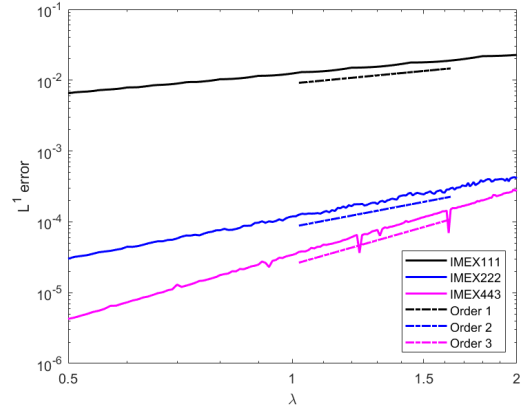


Fig. 6: Error plot for (75) with initial condition  $u_0(x, y, z) = \exp(-(x^2 + 2y^2 + 3z^2))$  using IMEX111, IMEX222 and IMEX443.

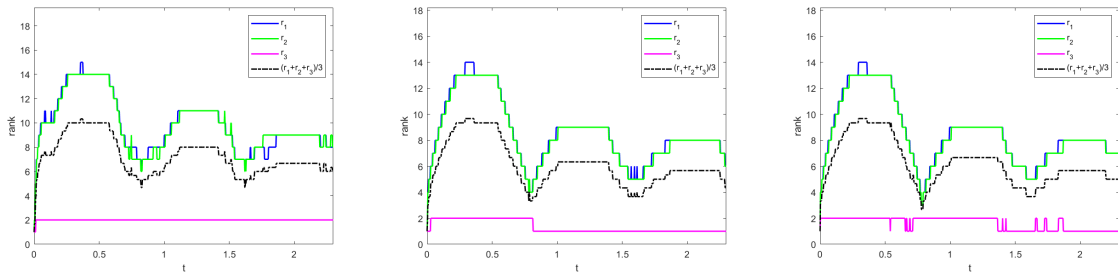


Fig. 7: The multilinear rank  $(r_1, r_2, r_3)$  and average of the multilinear rank  $(r_1 + r_2 + r_3)/3$  of the solution to (73) with initial condition  $u_0(x, y, z) = \exp(-(x^2 + 9y^2 + z^2))$  using IMEX111 (left), IMEX222 (middle) and IMEX443 (right).

$(1, 1, 1)$  as the solution (re)aligns with the axes at  $t = 0$ ,  $t = \pi/4$ ,  $t = \pi/2$ ,  $t = 3\pi/4$  and so forth. The rank in  $x$  and  $y$  should increase and decrease in between these time stamps as the solution rotates about  $\hat{z}$ , whereas the rank in  $z$  should remain one since the rotation is only occurring in the  $xy$ -plane. As seen in Figure 7, the RAIL scheme captures this behavior with IMEX111, IMEX222 and IMEX443. The decrease in the magnitude of the “humps” due to the slow diffusion is captured in all three plots, but IMEX443 does a slightly better job capturing the return to low-rank at times  $t = \pi/4$ ,  $t = \pi/2$  and  $t = 3\pi/4$ . For the rank plots, we used a mesh size  $N = 80$ , tolerance  $\varepsilon = 10^{-6}$ , and  $\lambda = 0.45$ . In our experiments, we observed that the solution only diffused and did not rotate when using large truncation tolerances and/or very small time-stepping sizes. This behavior was especially seen for the first-order IMEX111 time discretization, e.g., with  $\varepsilon = 10^{-6}$  and  $\lambda = 0.25$ ; decreasing the tolerance corrected this, as did increasing the time-stepping size. This observation was also seen with IMEX222, although only for extremely large tolerances, e.g.,  $\varepsilon = 10^{-1}$ , and extremely small time-stepping sizes. This behavior is known to occur with (low-order) BUG methods since the rotation is far from the tangent space and thus requires either a very small truncation tolerance or a large time-stepping size so that the rotation dynamics are more dominant; see Example 4.1 in [1].

#### Example 4 (Rigid body rotation with diffusion, about $\hat{x} + \hat{y} + \hat{z}$ )

$$u_t + (-y + z)u_x + (x - z)u_y + (-x + y)u_z = d(u_{xx} + u_{yy} + u_{zz}), \quad x, y, z \in (-2\pi, 2\pi) \quad (74)$$

where  $d = 1/12$  and the flow field describes rotation about the vector  $\hat{x} + \hat{y} + \hat{z}$ . Here, we test if the RAIL scheme accurately captures and maintains low-rank structure in solutions for which rotation occurs in all directions. We set the initial condition as  $u_0(x, y, z) = \exp(-2((x - \pi/2)^2 + (y + \pi/2)^2 + z^2))$ . This is a Gaussian distribution centered at the point  $(\pi/2, -\pi/2, 0)$  that rotates counterclockwise about the vector  $\hat{x} + \hat{y} + \hat{z}$  while slowly diffusing. As expected, Figure 8 shows the RAIL scheme maintains the

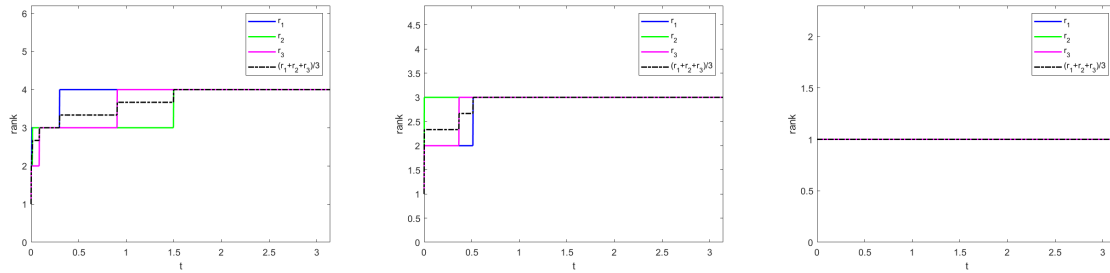


Fig. 8: The multilinear rank  $(r_1, r_2, r_3)$  and average of the multilinear rank  $(r_1 + r_2 + r_3)/3$  of the solution to (74) with initial condition  $u_0(x, y, z) = \exp(-2((x - \pi/2)^2 + (y + \pi/2)^2 + z^2))$  using IMEX111 (left), IMEX222 (middle) and IMEX443 (right).

low-rank structure in the solution for all three time discretizations, with IMEX443 performing the best. We used a mesh size  $N = 100$ , tolerance  $\varepsilon = 10^{-6}$ , and  $\lambda = 0.5$ .

### Example 5 (Rigid body rotation with diffusion and time-dependent flow field, about $\hat{z}$ )

$$u_t - tyu_x + txu_y = d(u_{xx} + u_{yy} + u_{zz}) + c(x, y, z, t), \quad x, y, z \in (-2\pi, 2\pi) \quad (75)$$

where the flow field describes rotation about the vector  $\hat{z}$  in which the speed starts at zero and increases linearly with  $t$ . To test the accuracy of the scheme, we use the manufactured solution  $u(x, y, z, t) = \exp(-(x^2 + 2y^2 + 3z^2 + 3dt))$  with  $d = 1/3$ , for which the source term  $c(x, y, z, t)$  is

$$c(x, y, z, t) = e^{-(x^2 + 2y^2 + 3z^2 + 3dt)} \left( -2txy - d(-9 + 4x^2 + 16y^2 + 36z^2) \right). \quad (76)$$

As seen in Figure 6, the expected accuracies are observed for the RAIL scheme when using IMEX111, IMEX222 and IMEX443. We used a mesh size  $N = 80$ , tolerance  $\varepsilon = 10^{-8}$ , final time  $T_f = 0.3$ , and  $\lambda$  ranging from 0.5 to 2. As with the time-independent flow field case, it is straightforward to write down a Tucker decomposition of (76).

To test the rank of the solution, we set  $d = 1/12$ ,  $c(x, y, z, t) = 0$ , double the speed of the rotation,

$$u_t - 2tyu_x + 2txu_y = \frac{1}{12}(u_{xx} + u_{yy} + u_{zz}), \quad x, y, z \in (-2\pi, 2\pi) \quad (77)$$

and set the initial condition to  $u_0(x, y, z) = \exp(-(x^2 + 9y^2 + z^2))$ . This is essentially the same rank test as was done for equation (73), but the speed has been scaled linear in  $t$  so that the solution will rotate counterclockwise by  $\pi/2$  radians (in the  $xy$ -plane) at  $t = \sqrt{\pi/2}$ , and  $\pi$  radians at  $t = \sqrt{\pi}$ . Theoretically, the exact multilinear rank should be  $(1, 1, 1)$  as the solution (re)aligns with the axes. The rank in  $x$  and  $y$  should increase and decrease in between these time stamps as the solution rotates about  $\hat{z}$ , whereas the rank in  $z$  should remain one since the rotation is only occurring in the  $xy$ -plane. As seen in Figure 9, the RAIL scheme captures this behavior with IMEX111, IMEX222 and IMEX443. The decrease in the magnitude of the ‘‘humps’’ due to the slow diffusion is captured in all three plots, but IMEX222 and IMEX443 do a slightly better job capturing the return to low-rank at times  $t = \sqrt{\pi/2}$  and  $t = \sqrt{\pi}$ . For the rank plots, we used a mesh size  $N = 100$ , tolerance  $\varepsilon = 10^{-6}$ , and  $\lambda = 1$ .

### Example 6 (Dougherty-Fokker-Planck equation)

$$f_t - ((v_x - \bar{v}_x)f)_x - ((v_y - \bar{v}_y)f)_y - ((v_z - \bar{v}_z)f)_z = D(f_{xx} + f_{yy} + f_{zz}), \quad v_x, v_y, v_z \in (-8, 8) \quad (78)$$

with gas constant  $R = 1/6$ , ion temperature  $T = 3$ , thermal velocity  $v_{th} = \sqrt{2RT} = \sqrt{2D} = 1$ , number density  $n = \pi^{3/2}$ , and bulk velocity  $\bar{\mathbf{v}} = \mathbf{0}$ . These quantities were chosen out of convenience so that the equilibrium solution is the Maxwellian distribution function

$$f_M^\infty(\mathbf{v}, t = 0) = \frac{n}{(2\pi RT)^{3/2}} \exp\left(-\frac{|\mathbf{v} - \bar{\mathbf{v}}|^2}{2RT}\right) = \exp(-|\mathbf{v}|^2). \quad (79)$$

Relaxation of the system is tested using the initial distribution function

$$f_0(\mathbf{v}) = f_{M1}(\mathbf{v}) + f_{M2}(\mathbf{v}), \quad (80)$$

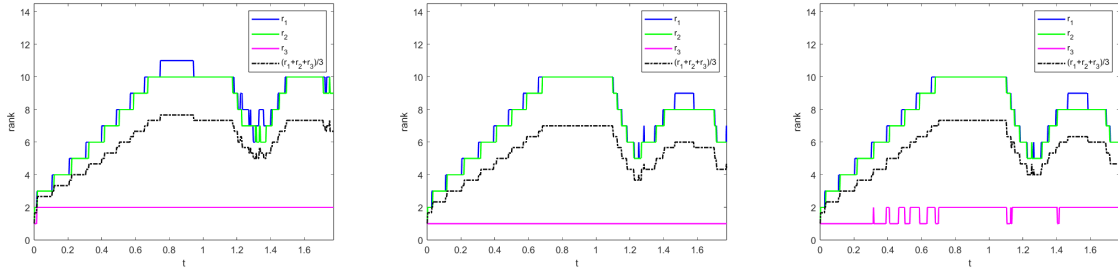


Fig. 9: The multilinear rank  $(r_1, r_2, r_3)$  and average of the multilinear rank  $(r_1 + r_2 + r_3)/3$  of the solution to (77) with initial condition  $u_0(x, y, z) = \exp(-(x^2 + 9y^2 + z^2))$  using IMEX111 (left), IMEX222 (middle) and IMEX443 (right).

where  $f_{M1}$  and  $f_{M2}$  are two randomly generated Maxwellians such that the total number density, bulk velocity, and temperature are  $n = \pi^{3/2}$ ,  $\bar{\mathbf{v}} = \mathbf{0}$ , and  $T = 3$ , respectively. As such, the solution will relax to Maxwellian (79) as  $t \rightarrow \infty$ . The number densities, bulk velocities, and temperatures that define the Maxwellians  $f_{M1}$  and  $f_{M2}$  are listed in Table 4.

	$f_{M1}$	$f_{M2}$
$n$	0.8037121822811545	4.764615814550553
$\bar{v}_x$	-0.3403147128006618	0.05740548475117823
$\bar{v}_y$	0	0
$\bar{v}_z$	0	0
$T$	0.1033754314349305	3.442950196134546

Table 4:  $n = \pi^{3/2}$ ,  $\bar{\mathbf{v}} = \mathbf{0}$ , and  $T = 3$ .

The initial condition (80) is rank-two, and the equilibrium solution (79) is rank-one. Similar to the diffusion equation example, the rank of the solution will immediately increase before quickly decreasing as the solution drives to relaxation. Figure 10 shows the RAIL scheme captures this behavior with all three time discretizations. IMEX443 better captures the decrease in rank ever so slightly, whereas IMEX111 takes a bit longer to decrease the rank of the solution. We used a mesh size  $N = 100$ , tolerance  $\varepsilon = 10^{-8}$ , and  $\lambda = 0.5$ .

When solving kinetic equations such as the Dougherty-Fokker-Planck equation, we often care about how well a numerical scheme preserves the equilibrium solution. That is, how well the numerical solution converges to the exact equilibrium solution in the  $L^1$  norm. Although the proposed RAIL scheme was not designed to preserve the equilibrium solution, we found that the RAIL scheme preserves the equilibrium solution up to the maximum of the tolerance  $\varepsilon$  and the error of the time discretization. Figure 11 shows the  $L^1$  decay of the solution using mesh size  $N = 100$ ,  $\lambda = 0.5$ , IMEX443 for the time discretization, and varying tolerances  $\varepsilon = 10^{-3}, 10^{-4}, 10^{-5}, 10^{-8}$ . Notice that the equilibrium solution is preserved up to the tolerance  $\varepsilon$ , but only until roughly  $10^{-6}$ . This is because the error from the IMEX443 RK method is roughly on the order of  $10^{-6}$ , despite the truncation tolerance being  $\varepsilon = 10^{-8}$ . We only present results using IMEX443 since results using IMEX111 or IMEX222 exhibit the same observation, except for the error of the time discretization being larger.

## 6 Conclusion

In this paper, we proposed a reduced augmentation implicit low-rank (RAIL) integrator for solving three-dimensional diffusion and advection-diffusion equations. The two-dimensional RAIL algorithm (matrix case) from previous work was extended to three-dimensions using a Tucker decomposition of the third-order tensor solution. The partial differential equations were fully discretized into tensor equations. By spanning the low-order prediction (or updated) bases with the bases from the previous RK stages in a reduced augmentation procedure, the tensor equations were projected onto a richer space that allowed high-order implicit and implicit-explicit methods to be used. Several numerical tests demonstrated the

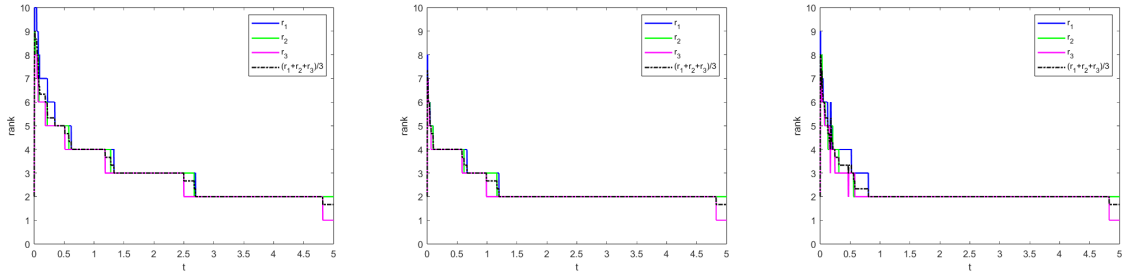


Fig. 10: The multilinear rank  $(r_1, r_2, r_3)$  and average of the multilinear rank  $(r_1 + r_2 + r_3)/3$  of the solution to (78) with initial condition (80) using IMEX111 (left), IMEX222 (middle) and IMEX443 (right).

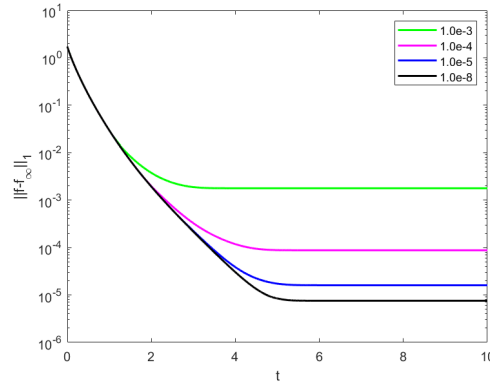


Fig. 11:  $L^1$  decay of the solution to (78) with initial condition (80) towards the equilibrium solution (79), that is,  $\|f - f_M^\infty\|_1$ . IMEX443 is used for the time discretization, along with varying tolerances  $\varepsilon = 10^{-3}, 10^{-4}, 10^{-5}, 10^{-8}$ .

proposed RAIL scheme's ability to achieve high-order accuracy and capture low-rank structure in solutions. This paper only considered three-dimensional equations, but the scheme can be generalized to higher dimensions using the Tucker decomposition. However, going to  $d$  dimensions increases the storage complexity of the Tucker decomposition to  $\mathcal{O}(r^d + dNR)$ , which becomes prohibitively large for  $d \geq 4$ . Ongoing and future work includes extending to hierarchical Tucker decomposition or other tree tensor networks to address dimensions  $d \geq 4$ , as well as deriving rigorous error bounds for the high-order RAIL scheme.

## Declarations

### Funding

The authors have no funding to report.

### Data Availability

The datasets and source code generated and analyzed in the current study are available upon request.

### Competing Interests

The authors have no competing interests.

Acknowledgments

Joseph Nakao wants to thank Valeria Simoncini for an insightful discussion at SIAM LA24 about her third-order tensor linear equation solver used in the proposed RAIL-3D integrator.

Appendix

Butcher tables for stiffly accurate DIRK methods [29]

Table 5: DIRK2

$\nu$	$\nu$	$0$
$1$	$1 - \nu$	$\nu$
	$1 - \nu$	$\nu$

Let  $\nu = 1 - \sqrt{2}/2$ .

Table 6: DIRK3

$\nu$	$\nu$	$0$	$0$
$\frac{1+\nu}{2}$	$\frac{1-\nu}{2}$	$\nu$	$0$
$1$	$\beta_1$	$\beta_2$	$\nu$
	$\beta_1$	$\beta_2$	$\nu$

Let  $\nu \approx 0.435866521508459$ ,  
 $\beta_1 = -\frac{3}{2}\nu^2 + 4\nu - \frac{1}{4}$ ,  
and  $\beta_2 = \frac{3}{2}\nu^2 - 5\nu + \frac{5}{4}$ .

Butcher tables for implicit-explicit Runge-Kutta methods [2]

Table 7: IMEX(1,1,1) – Implicit Table

$0$	$0$	$0$
$1$	$0$	$1$
	$0$	$1$

Table 8: IMEX(1,1,1) – Explicit Table

$0$	$0$	$0$
$1$	$1$	$0$
	$1$	$0$

Table 9: IMEX(2,2,2) – Implicit Table

$0$	$0$	$0$	$0$
$\nu$	$0$	$\nu$	$0$
$1$	$0$	$1 - \nu$	$\nu$
	$0$	$1 - \nu$	$\nu$

Table 10: IMEX(2,2,2) – Explicit Table

$0$	$0$	$0$	$0$
$\nu$	$\nu$	$0$	$0$
$1$	$\delta$	$1 - \delta$	$0$
	$\delta$	$1 - \delta$	$0$

Let  $\nu = 1 - \sqrt{2}/2$  and  $\delta = 1 - 1/(2\nu)$ .

Table 11: IMEX(4,4,3) – Implicit Table

$0$	$0$	$0$	$0$	$0$	$0$
$1/2$	$0$	$1/2$	$0$	$0$	$0$
$2/3$	$0$	$1/6$	$1/2$	$0$	$0$
$1/2$	$0$	$-1/2$	$1/2$	$1/2$	$0$
$1$	$0$	$3/2$	$-3/2$	$1/2$	$1/2$
	$0$	$3/2$	$-3/2$	$1/2$	$1/2$

Table 12: IMEX(4,4,3) – Explicit Table

$0$	$0$	$0$	$0$	$0$	$0$
$1/2$	$1/2$	$0$	$0$	$0$	$0$
$2/3$	$11/18$	$1/18$	$0$	$0$	$0$
$1/2$	$5/6$	$-5/6$	$1/2$	$0$	$0$
$1$	$1/4$	$7/4$	$3/4$	$-7/4$	$0$
	$1/4$	$7/4$	$3/4$	$-7/4$	$0$

RAIL-3D algorithms

This appendix includes the algorithms for the reduced augmentation procedure (Algorithm 1), and the high-order RAIL-3D scheme (Algorithm 2). Since the reduced augmentation procedure is used both before the  $K_1$ - $K_2$ - $K_3$  and  $G$  steps, we specify the slightly different inputs and outputs. We only include

**Algorithm 1** Reduced augmentation procedure at the  $k$ th Runge-Kutta stage

---

**Input (K<sub>1</sub>-K<sub>2</sub>-K<sub>3</sub> steps):**  $\{\mathbf{V}_x^{\dagger,(k)}, \mathbf{V}_x^{(k-1)}, \dots, \mathbf{V}_x^{(0)}\}, \{\mathbf{V}_y^{\dagger,(k)}, \mathbf{V}_y^{(k-1)}, \dots, \mathbf{V}_y^{(0)}\}, \{\mathbf{V}_z^{\dagger,(k)}, \mathbf{V}_z^{(k-1)}, \dots, \mathbf{V}_z^{(0)}\}$   
**Output (K<sub>1</sub>-K<sub>2</sub>-K<sub>3</sub> steps):**  $\mathbf{V}_x^{*(k)}, \mathbf{V}_y^{*(k)}, \mathbf{V}_z^{*(k)}$   
**Input (G step):**  $\{\mathbf{V}_x^{\dagger,(k)}, \mathbf{V}_x^{(k-1)}, \dots, \mathbf{V}_x^{(0)}\}, \{\mathbf{V}_y^{\dagger,(k)}, \mathbf{V}_y^{(k-1)}, \dots, \mathbf{V}_y^{(0)}\}, \{\mathbf{V}_z^{\dagger,(k)}, \mathbf{V}_z^{(k-1)}, \dots, \mathbf{V}_z^{(0)}\}$   
**Output (G step):**  $\hat{\mathbf{V}}_x^{(k)}, \hat{\mathbf{V}}_y^{(k)}, \hat{\mathbf{V}}_z^{(k)}$

---

1: Augment the bases.

If K<sub>1</sub>-K<sub>2</sub>-K<sub>3</sub> Steps:

[Qx,Rx] = qr([Vx\_dagger,Vx\_{k-1},...,Vx\_1,Vx\_0],0);  
 [Qy,Ry] = qr([Vy\_dagger,Vy\_{k-1},...,Vy\_1,Vy\_0],0);  
 [Qz,Rz] = qr([Vz\_dagger,Vz\_{k-1},...,Vz\_1,Vz\_0],0);

If G Step:

[Qx,Rx] = qr([Vx\_ddagger,Vx\_{k-1},...,Vx\_1,Vx\_0],0);  
 [Qy,Ry] = qr([Vy\_ddagger,Vy\_{k-1},...,Vy\_1,Vy\_0],0);  
 [Qz,Rz] = qr([Vz\_ddagger,Vz\_{k-1},...,Vz\_1,Vz\_0],0);

2: Reduce with respect to tolerance  $1.0e-12$ .

[Vx\_temp,Sx\_temp,~] = svd(Rx,0);  
 [Vy\_temp,Sy\_temp,~] = svd(Ry,0);  
 [Vz\_temp,Sz\_temp,~] = svd(Rz,0);  
 rx = find(diag(Sx\_temp)>1.0e-12,1,'last');  
 ry = find(diag(Sy\_temp)>1.0e-12,1,'last');  
 rz = find(diag(Sz\_temp)>1.0e-12,1,'last');

3: Keep the corresponding left singular vectors.

If K<sub>1</sub>-K<sub>2</sub>-K<sub>3</sub> Steps:

Vx\_star = Qx\*Vx\_temp(:,1:rx);  
 Vy\_star = Qy\*Vy\_temp(:,1:ry);  
 Vz\_star = Qz\*Vz\_temp(:,1:rz);

If G Step:

R = min(max([rx,ry,rz]),min([length(Rx),length(Ry),length(Rz)])); Need  $r_x = r_y = r_z$  for direct solver.  
 Vx\_hat = Qx\*Vx\_star(:,1:R);  
 Vy\_hat = Qy\*Vy\_star(:,1:R);  
 Vz\_hat = Qz\*Vz\_star(:,1:R);

---

**Algorithm 2** The RAIL-3D algorithm for advection-diffusion equations using IMEX RK methods

**Input:**  $\mathbf{V}_x^n, \mathbf{V}_y^n, \mathbf{V}_z^n, \mathcal{G}^n$  and  $(r_x^n, r_y^n, r_z^n)$

**Output:**  $\mathbf{V}_x^{n+1}, \mathbf{V}_y^{n+1}, \mathbf{V}_z^{n+1}, \mathcal{G}^{n+1}$  and  $(r_x^{n+1}, r_y^{n+1}, r_z^{n+1})$

for each RK stage  $k = 1, 2, \dots, s$  do

1: Compute the predictions  $\mathbf{V}_x^{\dagger,(k)}, \mathbf{V}_y^{\dagger,(k)}$  and  $\mathbf{V}_z^{\dagger,(k)}$ ; not needed for first stage.

2: Construct the projection bases  $\mathbf{V}_x^{*(k)}, \mathbf{V}_y^{*(k)}$  and  $\mathbf{V}_z^{*(k)}$  using Algorithm 1. Algorithm 1 is not needed in the first-order scheme since  $\mathbf{V}^{*(k)} = \mathbf{V}^n$ .

3: for each dimension  $i \in \{x, y, z\}$  do

    Compute  $\mathbf{W}_i^{(k-1)}$ , e.g., (62). This requires computing the Tucker decomposition (54) at the previous RK stages.

    Solve the  $K_i$  equation, e.g., (45) for  $\mathbf{K}_i^{(k)}$ .

    Compute and store the update basis  $\mathbf{V}_i^{\dagger,(k)}$ .

    [Vi\_ddagger,~] = qr(Ki,0);

4: Construct the bases  $\hat{\mathbf{V}}_x^{(k)}, \hat{\mathbf{V}}_y^{(k)}$  and  $\hat{\mathbf{V}}_z^{(k)}$  using Algorithm 1.

5: Compute  $\mathcal{B}^{(k-1)}$  (63), and solve the G equation (48) for  $\mathcal{G}^{(k)}$ . We use the direct solver in Corollary 1.

6: Truncate the solution using the truncated HOSVD/MLSVD. We use the `mlsvd` function in Tensorlab [63, 64].

7: Store  $\mathbf{V}_x^{(k)}, \mathbf{V}_y^{(k)}, \mathbf{V}_z^{(k)}$  and  $\mathcal{G}^{(k)}$ .

Store the final solution  $\mathbf{V}_x^{n+1}, \mathbf{V}_y^{n+1}, \mathbf{V}_z^{n+1}, \mathcal{G}^{n+1}$  and  $(r_x^{n+1}, r_y^{n+1}, r_z^{n+1})$ .

---

the algorithm for the high-order implicit-explicit RAIL-3D scheme since the implicit RAIL-3D scheme follows similarly. Algorithm 2 assumes IMEX RK methods that use stiffly accuracy DIRK methods for the implicit treatment.

**References**

- [1] Daniel Appelö and Yingda Cheng. “Robust implicit adaptive low rank time-stepping methods for matrix differential equations”. In: *Journal of Scientific Computing* 102.3 (2025), p. 81.

- [2] U. M. Ascher, S. J. Ruuth, and R. J. Spiteri. “Implicit-explicit Runge-Kutta methods for time-dependent partial differential equations”. In: *Applied Numerical Mathematics* 25.2-3 (1997), pp. 151–167.
- [3] Richard H. Bartels and George W Stewart. “Solution of the matrix equation  $AX + XB = C$  [F4]”. In: *Communications of the ACM* 15.9 (1972), pp. 820–826.
- [4] Benjamin Carrel. *Randomised methods for dynamical low-rank approximation*. 2024. arXiv: [2410.17091](https://arxiv.org/abs/2410.17091) [math.NA]. URL: <https://arxiv.org/abs/2410.17091>.
- [5] Gianluca Ceruti, Jonas Kusch, and Christian Lubich. “A parallel rank-adaptive integrator for dynamical low-rank approximation”. In: *SIAM Journal on Scientific Computing* 46.3 (2024), B205–B228.
- [6] Gianluca Ceruti, Jonas Kusch, and Christian Lubich. “A rank-adaptive robust integrator for dynamical low-rank approximation”. In: *BIT Numerical Mathematics* 62.4 (2022), pp. 1149–1174.
- [7] Gianluca Ceruti and Christian Lubich. “An unconventional robust integrator for dynamical low-rank approximation”. In: *BIT Numerical Mathematics* 62.1 (2022), pp. 23–44.
- [8] Gianluca Ceruti, Christian Lubich, and Hanna Walach. “Time integration of tree tensor networks”. In: *SIAM Journal on Numerical Analysis* 59.1 (2021), pp. 289–313.
- [9] Gianluca Ceruti et al. “A robust second-order low-rank BUG integrator based on the midpoint rule”. In: *BIT Numerical Mathematics* 64.3 (2024), p. 30.
- [10] Lieven De Lathauwer, Bart De Moor, and Joos Vandewalle. “A multilinear singular value decomposition”. In: *SIAM journal on Matrix Analysis and Applications* 21.4 (2000), pp. 1253–1278.
- [11] Alec Dektor. “Collocation methods for nonlinear differential equations on low-rank manifolds”. In: *Linear Algebra and its Applications* 705 (2025), pp. 143–184.
- [12] Alec Dektor and Lukas Einkemmer. “Interpolatory dynamical low-rank approximation for the 3+3d Boltzmann-BGK equation”. In: *arXiv preprint arXiv:2411.15990* (2024).
- [13] Zhiyan Ding, Lukas Einkemmer, and Qin Li. “Dynamical low-rank integrator for the linear Boltzmann equation: error analysis in the diffusion limit”. In: *SIAM Journal on Numerical Analysis* 59.4 (2021), pp. 2254–2285.
- [14] Sergey V Dolgov, Alexander P Smirnov, and EE Tyrtysnikov. “Low-rank approximation in the numerical modeling of the Farley–Buneman instability in ionospheric plasma”. In: *Journal of Computational Physics* 263 (2014), pp. 268–282.
- [15] M Donello et al. “Oblique projection for scalable rank-adaptive reduced-order modelling of nonlinear stochastic partial differential equations with time-dependent bases”. In: *Proceedings of the Royal Society A* 479.2278 (2023), p. 20230320.
- [16] Virginie Ehrlacher and Damiano Lombardi. “A dynamical adaptive tensor method for the Vlasov–Poisson system”. In: *Journal of Computational Physics* 339 (2017), pp. 285–306.
- [17] Lukas Einkemmer, Jingwei Hu, and Yubo Wang. “An asymptotic-preserving dynamical low-rank method for the multi-scale multi-dimensional linear transport equation”. In: *Journal of Computational Physics* 439 (2021), p. 110353.
- [18] Lukas Einkemmer et al. “A review of low-rank methods for time-dependent kinetic simulations”. In: *arXiv preprint arXiv:2412.05912* (2024).
- [19] Hamad El Kahza et al. “Krylov-based adaptive-rank implicit time integrators for stiff problems with application to nonlinear Fokker-Planck kinetic models”. In: *Journal of Computational Physics* 518 (2024), p. 113332.
- [20] Hamad El Kahza et al. “Sylvester-Preconditioned Adaptive-Rank Implicit Time Integrators for Advection-Diffusion Equations with Inhomogeneous Coefficients”. In: *arXiv preprint arXiv:2410.19662* (2024).
- [21] Martin Frank, Jonas Kusch, and Chinmay Patwardhan. “Asymptotic-preserving and energy stable dynamical low-rank approximation for thermal radiative transfer equations”. In: *Multiscale Modeling & Simulation* 23.1 (2025), pp. 278–312.
- [22] Behzad Ghahremani and Hessam Babae. “A DEIM Tucker tensor cross algorithm and its application to dynamical low-rank approximation”. In: *Computer Methods in Applied Mechanics and Engineering* 423 (2024), p. 116879.
- [23] Behzad Ghahremani and Hessam Babae. “Cross interpolation for solving high-dimensional dynamical systems on low-rank Tucker and tensor train manifolds”. In: *Computer Methods in Applied Mechanics and Engineering* 432 (2024), p. 117385.
- [24] Gene Golub, Stephen Nash, and Charles Van Loan. “A Hessenberg-Schur method for the problem  $AX + XB = C$ ”. In: *IEEE Transactions on Automatic Control* 24.6 (1979), pp. 909–913.

- [25] Lars Grasedyck, Daniel Kressner, and Christine Tobler. “A literature survey of low-rank tensor approximation techniques”. In: *GAMM-Mitteilungen* 36.1 (2013), pp. 53–78.
- [26] Wei Guo and Jing-Mei Qiu. “A conservative low rank tensor method for the Vlasov dynamics”. In: *SIAM Journal on Scientific Computing* 46.1 (2024), A232–A263.
- [27] Wei Guo and Jing-Mei Qiu. “A Local Macroscopic Conservative (LoMaC) low rank tensor method for the Vlasov dynamics”. In: *Journal of Scientific Computing* 101.3 (2024), p. 61.
- [28] Wolfgang Hackbusch and Stefan Kühn. “A new scheme for the tensor representation”. In: *Journal of Fourier analysis and applications* 15.5 (2009), pp. 706–722.
- [29] E. Hairer and G. Wanner. *Solving Ordinary Differential Equations II, Stiff and Differential-Algebraic Problems*. Springer Berlin Heidelberg, 1996.
- [30] Arie Kapteyn, Heinz Neudecker, and Tom Wansbeek. “An approach to n-mode components analysis”. In: *Psychometrika* 51 (1986), pp. 269–275.
- [31] Othmar Koch and Christian Lubich. “Dynamical low-rank approximation”. In: *SIAM Journal on Matrix Analysis and Applications* 29.2 (2007), pp. 434–454.
- [32] Othmar Koch and Christian Lubich. “Dynamical tensor approximation”. In: *SIAM Journal on Matrix Analysis and Applications* 31.5 (2010), pp. 2360–2375.
- [33] Tamara G Kolda and Brett W Bader. “Tensor decompositions and applications”. In: *SIAM review* 51.3 (2009), pp. 455–500.
- [34] Katharina Kormann. “Low-rank tensor discretization for high-dimensional problems”. In: *Vorlesung (SS 2017)* (2017).
- [35] Daniel Kressner and Lana Perisa. “Recompression of Hadamard products of tensors in Tucker format”. In: *SIAM Journal on Scientific Computing* 39.5 (2017), A1879–A1902.
- [36] Daniel Kressner and Petar Sirković. “Truncated low-rank methods for solving general linear matrix equations”. In: *Numerical Linear Algebra with Applications* 22.3 (2015), pp. 564–583.
- [37] Patrick Kürschner. “Efficient low-rank solution of large-scale matrix equations”. PhD thesis. Shaker Verlag Aachen, 2016.
- [38] Jonas Kusch. “Second-order robust parallel integrators for dynamical low-rank approximation”. In: *arXiv preprint arXiv:2403.02834* (2024).
- [39] Hei Yin Lam, Gianluca Ceruti, and Daniel Kressner. “Randomized low-rank runge-kutta methods”. In: *arXiv preprint arXiv:2409.06384* (2024).
- [40] Namgil Lee and Andrzej Cichocki. “Fundamental tensor operations for large-scale data analysis in tensor train formats”. In: *arXiv preprint arXiv:1405.7786* (2014).
- [41] Shun Li, Yan Jiang, and Yingda Cheng. “High-Order Implicit Low-Rank Method with Spectral Deferred Correction for Matrix Differential Equations”. In: *arXiv preprint arXiv:2412.09400* (2024).
- [42] Christian Lubich and Ivan V Oseledets. “A projector-splitting integrator for dynamical low-rank approximation”. In: *BIT Numerical Mathematics* 54.1 (2014), pp. 171–188.
- [43] Christian Lubich, Bart Vandereycken, and Hanna Walach. “Time integration of rank-constrained Tucker tensors”. In: *SIAM Journal on Numerical Analysis* 56.3 (2018), pp. 1273–1290.
- [44] Christian Lubich et al. “Dynamical approximation by hierarchical Tucker and tensor-train tensors”. In: *SIAM Journal on Matrix Analysis and Applications* 34.2 (2013), pp. 470–494.
- [45] Shixu Meng, Daniel Appelo, and Yingda Cheng. “Preconditioning low rank generalized minimal residual method (gmres) for implicit discretizations of matrix differential equations”. In: *arXiv preprint arXiv:2410.07465* (2024).
- [46] Mohammad Hossein Naderi and Hessam Babae. “Adaptive sparse interpolation for accelerating nonlinear stochastic reduced-order modeling with time-dependent bases”. In: *Computer Methods in Applied Mechanics and Engineering* 405 (2023), p. 115813.
- [47] Mohammad Hossein Naderi and Hessam Babae. “CUR-Based Implicit Integration of Random Partial Differential Equations on Low-Rank Manifolds”. In: *APS Division of Fluid Dynamics Meeting Abstracts*. 2024, pp. X11–007.
- [48] Joseph Nakao, Jing-Mei Qiu, and Lukas Einkemmer. “Reduced Augmentation Implicit Low-rank (RAIL) integrators for advection-diffusion and Fokker-Planck models”. In: *To appear in SIAM Journal on Scientific Computing, arXiv preprint arXiv:2311.15143* (2023).
- [49] Fabio Nobile and Sébastien Riffaud. “Robust high-order low-rank BUG integrators based on explicit Runge-Kutta methods”. In: *arXiv preprint arXiv:2502.07040* (2025).
- [50] Ivan V Oseledets. “Tensor-train decomposition”. In: *SIAM Journal on Scientific Computing* 33.5 (2011), pp. 2295–2317.
- [51] Stefan Ragnarsson. “Structured tensor computations: Blocking, symmetries and Kronecker factorizations”. PhD thesis. Cornell University, 2012.

- 
- [52] Abram Rodgers, Alec Dektor, and Daniele Venturi. “Adaptive integration of nonlinear evolution equations on tensor manifolds”. In: *Journal of Scientific Computing* 92.2 (2022), p. 39.
- [53] Abram Rodgers and Daniele Venturi. “Implicit integration of nonlinear evolution equations on tensor manifolds”. In: *Journal of Scientific Computing* 97.2 (2023), p. 33.
- [54] Abram Rodgers and Daniele Venturi. “Step-truncation integrators for evolution equations on low-rank tensor manifolds”. In: *CoRR* (2020).
- [55] Abram Rodgers and Daniele Venturi. “Tensor approximation of functional differential equations”. In: *Physical Review E* 110.1 (2024), p. 015310.
- [56] William A Sands et al. “High-order adaptive rank integrators for multi-scale linear kinetic transport equations in the hierarchical tucker format”. In: *arXiv preprint arXiv:2406.19479* (2024).
- [57] Axel Séguin, Gianluca Ceruti, and Daniel Kressner. “From low-rank retractions to dynamical low-rank approximation and back”. In: *BIT Numerical Mathematics* 64.3 (2024), p. 25.
- [58] V Simoncini. “Numerical solution of a class of third order tensor linear equations”. In: *Bollettino dell’Unione Matematica Italiana* 13.3 (2020), pp. 429–439.
- [59] Marco Sutti and Bart Vandereycken. “Implicit low-rank Riemannian schemes for the time integration of stiff partial differential equations”. In: *Journal of Scientific Computing* 101.1 (2024), p. 3.
- [60] Lloyd N Trefethen. *Spectral methods in MATLAB*. SIAM, 2000.
- [61] Ledyard R Tucker. “Implications of factor analysis of three-way matrices for measurement of change”. In: *Problems in measuring change* 15.122-137 (1963), p. 3.
- [62] Ledyard R Tucker. “Some mathematical notes on three-mode factor analysis”. In: *Psychometrika* 31.3 (1966), pp. 279–311.
- [63] Nico Vervliet, Otto Debals, and Lieven De Lathauwer. “Tensorlab 3.0—numerical optimization strategies for large-scale constrained and coupled matrix/tensor factorization”. In: *2016 50th Asilomar Conference on Signals, Systems and Computers*. IEEE, 2016, pp. 1733–1738.
- [64] Nico Vervliet et al. “Tensorlab 3.0”. In: *Available online: <http://www.tensorlab.net>* (2016).
- [65] Haijin Wang, Chi-Wang Shu, and Qiang Zhang. “Stability and error estimates of local discontinuous Galerkin methods with implicit-explicit time-marching for advection-diffusion problems”. In: *SIAM Journal on Numerical Analysis* 53.1 (2015), pp. 206–227.